R. & M. No. 3739

R. & M. No. 3739

MINISTRY OF DEFENCE (PROCUREMENT EXECUTIVE)

AERONAUTICAL RESEARCH COUNCIL

REPORTS AND MEMORANDA

An Integral Prediction Method for Three-Dimensional Compressible Turbulent Boundary Layers

By P. D. Smith

Aerodynamics Dept., R.A.E., Bedford

LONDON: HER MAJESTY'S STATIONERY OFFICE

1974

PRICE £2 NET

An Integral Prediction Method for Three-Dimensional Compressible Turbulent Boundary Layers

By P. D. SMITH

Aerodynamics Dept., R.A.E., Bedford

Reports and Memoranda No. 3739*
December, 1972

Summary

A calculation method has been developed which uses the compressible forms of the boundary-layer momentum integral and entrainment equations in a general, curvilinear surface coordinate system in which the axes are not necessarily orthogonal. Both the Mager and Johnston representations of the crossflow velocity profile can be used. The set of equations used is hyperbolic and is solved numerically by a simple explicit finite difference method. In cases where the metric coefficients of the coordinate system used are not known analytically a method is given for obtaining them from the Cartesian coordinates of the surface. A method is also presented for determining the external velocity field from a given pressure distribution. Comparisons are given of predictions of the boundary-layer method with the experimental results of Johnston, Vermeulen, East, van den Berg and Elsenaar, and Hall and Dickens. These results, involving five different coordinate systems, were all obtained using the same computer program.

* Replaces R.A.E. Technical Report 72228—A.R.C. 34 452.

LIST OF CONTENTS

1. Introduction

Three-dimensional turbulent boundary layers are in all probability the most commonly occurring form of boundary-layer flows. They occur, for example, on swept wings and on bodies at incidence. Prediction of such flows is of considerable practical importance and here a method is given for the calculation of the three-dimensional compressible boundary-layer development over an insulated surface.

Prediction methods for two-dimensional turbulent boundary layers are generally of two forms; finite difference methods in which the governing partial differential equations are solved numerically and integral methods in which the partial differential equations are reduced, by an integration in the direction normal to the surface, to a set of ordinary differential equations which are then solved numerically. Both forms involve considerable empiricism to render the equations used determinate. Integral methods are generally much faster.

For three-dimensional flows these two forms remain, although in this case the integral methods involve partial differential equations but with only two independent variables, rather than the three of finite difference methods, so that the former's speed advantage should to some extent be retained.

Integral prediction methods for three-dimensional turbulent boundary layers have usually made use of a streamline coordinate system which consists of two families of mutually-orthogonal curves on the body surface. One family is formed by the projections, onto the surface, of streamlines just external to the boundary layer. The direction of an external streamline is called the streamwise direction and boundary-layer flow normal to an external streamline and parallel to the surface is called crossflow. The assumption is then made that the streamwise flow is similar to that of a corresponding two-dimensional boundary layer.

Myring[1] has shown, however, that we may make use of the observed similarities with two-dimensional flows even when an axis system is adopted which is not based on the external streamlines. The abandonment of the streamline coordinate system yields two considerable advantages; firstly, the coordinate system can remain unchanged despite changes in the external flow about the body and secondly, the axis system may be chosen to give an even coverage of the body surface.

Myring developed a calculation method which used the momentum integral and entrainment equations in a general coordinate system. Here we extend this method to compressible flow over adiabatic walls and use a numerical method of solution which takes account of the hyperbolic nature of the equations involved. The method uses a non-orthogonal curvilinear coordinate system on the body surface. In cases where the metric coefficients of this coordinate system are not known a numerical technique is presented for obtaining them from the Cartesian coordinates of the surface.

The use of a general coordinate system results in an extremely flexible computer program. The five comparisons of the boundary-layer method with experimental results given here, which involved five different coordinate systems, were all obtained using the same computer program. In four of these cases the comparison with experimental results is encouraging, in the remaining case the discrepancies between experiment and calculation are unresolved.

The boundary-layer method requires that the velocity external to the boundary layer be known. When, as is often the case, only a pressure distribution is available, the velocity components may be obtained from this by means of a calculation scheme which is given here. This calculation proceeds simultaneously with the boundary-layer calculation.

2. Governing Equations

2.1. Momentum Integral Equations

The axis system used here is that introduced by Myring[1] and is shown in Fig. 1. The z-axis is normal to the surface and x and y form a non-orthogonal curvilinear mesh on the body surface. Velocities in the x, y and z directions are denoted by u, v and w respectively. An element of length ds on the body surface is given by

$$ds^2 = h_1^2\, dx^2 + h_2^2\, dy^2 + 2g\, dx\, dy, \tag{1}$$

where $g \equiv h_1 h_2 \cos\lambda$.

The boundary-level momentum integral equations in this coordinate system are given by Myring as

$$\frac{1}{h_1}\frac{\partial\Theta_{11}}{\partial x} + \Theta_{11}\left\{\frac{(2-M^2)}{h_1}\frac{1}{u_e}\frac{\partial u_e}{\partial x} + \frac{1}{q}\frac{\partial}{\partial x}\left(\frac{q}{h_1}\right) + k_1\right\} + \frac{1}{h_2}\frac{\partial\Theta_{12}}{\partial y}$$

$$+ \Theta_{12}\left\{\frac{(2 - M^2)}{h_2}\frac{1}{u_e}\frac{\partial u_e}{\partial y} + \frac{1}{q}\frac{\partial}{\partial y}\right)\left(\frac{q}{h_2}\right) + k_3\right\} + \Delta_1\left\{\frac{1}{h_1}\frac{1}{u_e}\frac{\partial u_1}{\partial x} + k_1\frac{u_1}{u_e}\right\} +$$

$$+ \Delta_2\left\{\frac{1}{h_2}\frac{1}{u_e}\frac{\partial u_1}{\partial y} + k_2\frac{v_1}{u_e} + k_3\frac{u_1}{u_e}\right\} + \Theta_{22}k_2 = \frac{C_{f1}}{2} \tag{2}$$

and

$$\frac{1}{h_1}\frac{\partial \Theta_{21}}{\partial x} + \Theta_{21}\left\{\frac{(2 - M^2)}{h_1}\frac{1}{u_e}\frac{\partial u_e}{\partial x} + \frac{1}{q}\frac{\partial}{\partial x}\left(\frac{q}{h_1}\right) + l_3\right\} + \frac{1}{h_2}\frac{\partial \Theta_{22}}{\partial y} +$$

$$+ \Theta_{22}\left\{\frac{(2 - M^2)}{h_2}\frac{1}{u_e}\frac{\partial u_e}{\partial y} + \frac{1}{q}\frac{\partial}{\partial y}\left(\frac{q}{h_2}\right) + l_2\right\} + \Delta_1\left\{\frac{1}{h_1}\frac{1}{u_e}\frac{\partial v_1}{\partial x} + l_1\frac{u_1}{u_e} + l_3\frac{v_1}{u_e}\right\} +$$

$$+ \Delta_2\left\{\frac{1}{h_2}\frac{1}{u_e}\frac{\partial v_1}{\partial y} + l_2\frac{v_1}{u_e}\right\} + \Theta_{11}l_1 = \frac{C_{f2}}{2}, \tag{3}$$

where M is the Mach number at the edge of the boundary layer and C_{f1} and C_{f2} are the skin-friction coefficients in the x and y directions respectively. The velocity components in the x, y directions at the edge of the boundary layer are denoted by u_1, v_1 and the resultant velocity at the boundary-layer edge is denoted by u_e where

$$u_e^2 = u_1^2 + v_1^2 + 2\cos\lambda u_1 v_1. \tag{4}$$

The various integral thicknesses appearing in equations (2) and (3) are defined in Appendix A together with the quantities $k_1, k_2, k_3, l_1, l_2, l_3$ and q.

2.2. Entrainment Equation

The entrainment or continuity integral equation is given by Myring as

$$\frac{1}{\rho_e u_e q}\left[\frac{\partial}{\partial x}\left\{\frac{\rho_e q}{h_1}(u_1\delta - u_e\Delta_1)\right\} + \frac{\partial}{\partial y}\left\{\frac{\rho_e q}{h_2}(v_1\delta - u_e\Delta_2)\right\}\right] = \frac{1}{u_e}\left[\frac{u_1}{h_1}\frac{\partial \delta}{\partial x} + \frac{v_1}{h_2}\frac{\partial \delta}{\partial y} - w_1\right] = F, \tag{5}$$

where ρ_e is the density at the boundary-layer edge and δ denotes the boundary layer thickness. F denotes the non-dimensional rate of change of mass flow in the boundary layer. The usefulness of equation (5) depends on the assumption that F can be prescribed as an empirical function of local boundary-layer properties.

2.3. Displacement Thickness and the Equivalent Source Distribution

Equation (5) may be rearranged as

$$w_1 = -\frac{\delta}{\rho_e q}\left[\frac{\partial}{\partial x}\left(\frac{\rho_e q u_1}{h_1}\right) + \frac{\partial}{\partial y}\left(\frac{\rho_e q v_1}{h_2}\right)\right] + \frac{1}{\rho_e q}\left[\frac{\partial}{\partial x}\left(\frac{\rho_e q u_e \Delta_1}{h_1}\right) + \frac{\partial}{\partial y}\left(\frac{\rho_e q u_e \Delta_2}{h_2}\right)\right]. \tag{6}$$

The first term on the right-hand side of this equation is that which would alone be present, at a distance δ from the surface, in the irrotational flow around the body. The second term is the additional outflow due to the boundary layer and is 'as if' there were a source distribution on the surface of strength m per unit area where

$$m = \frac{1}{\rho_e q}\left[\frac{\partial}{\partial x}\left(\frac{\rho_e q u_e \Delta_1}{h_1}\right) + \frac{\partial}{\partial y}\left(\frac{\rho_e q u_e \Delta_2}{h_2}\right)\right]. \tag{7}$$

The irrotational flow past the body plus a displacement surface of local thickness δ^* yields, at $z = \delta$, a value of w given by

$$w_1 = -\frac{(\delta - \delta^*)}{\rho_e q}\left[\frac{\partial}{\partial x}\left(\frac{\rho_e q u_1}{h_1}\right) + \frac{\partial}{\partial y}\left(\frac{\rho_e q v_1}{h_2}\right)\right] + \frac{u_1}{h_1}\frac{\partial \delta^*}{\partial x} + \frac{v_1}{h_2}\frac{\partial \delta^*}{\partial y}. \tag{8}$$

Equating equations (6) and (8) we obtain

$$\frac{\partial}{\partial x}\left(\frac{\rho_e q u_1 \delta^*}{h_1}\right) + \frac{\partial}{\partial y}\left(\frac{\rho_e q v_1 \delta^*}{h_2}\right) = \frac{\partial}{\partial x}\left(\frac{\rho_e q u_e \Delta_1}{h_1}\right) + \frac{\partial}{\partial y}\left(\frac{\rho_e q u_e \Delta_2}{h_2}\right), \tag{9}$$

which may be solved for δ^* once Δ_1 and Δ_2 have been determined. Equation (9) is Myring's equation (22) with an error in sign corrected.

2.4. Introduction of Streamwise Integral Quantities

The equations (2), (3) and (5) form the basis of the calculation method, but to proceed further we must reduce the number of unknowns contained therein to three. This is done, as shown below, by using assumed forms of velocity profiles together with skin friction and entrainment relationships. Empirical knowledge of these parameters is restricted to the streamline coordinate system in which one family of a set of mutually orothogonal coordinate curves is formed by the projections, onto the surface, of streamlines just external to the boundary layer. The direction of an external streamline is called the streamwise direction and boundary-layer flow normal to an external streamline and parallel to the surface is called crossflow. It is convenient, therefore, to express all the integral thicknesses so far introduced in terms of the more familiar integral thicknesses in the streamwise and crossflow directions. Expressions relating Θ_{11}, Θ_{12}, Θ_{21}, Δ_1 and Δ_2 in terms of θ_{11}, θ_{12}, θ_{21}, δ_1, δ_2, λ and α are therefore given in Appendix B. Here lower case θs and δs denote the integral thicknesses in the streamwise and crossflow direction, α is the angle between the x-axis and the external streamline and λ is the angle between the x- and y-axes.

3. Introduction of Empirical Relationships

3.1. Streamwise Velocity Profiles

We define the shape parameters H, $\bar{H}$ and H_1 as

$$H = \frac{\delta_1}{\theta_{11}},$$

$$\bar{H} = \frac{1}{\theta_{11}} \int_0^\delta \frac{\rho}{\rho_e}\left(1 - \frac{U}{u_e}\right) dz \tag{10}$$

and

$$H_1 = \frac{(\delta - \delta_1)}{\theta_{11}}.$$

We now assume, as was done in Ref. 2, that the streamwise velocity profiles are of the form suggested by Spence for two-dimensional flow, that is

$$\frac{U}{u_e} = \left(\frac{Z}{Z_\delta}\right)^n \tag{11}$$

where

$$Z = \int_0^z \frac{\rho}{\rho_e} dz \quad \text{and} \quad Z_\delta = \int_0^\delta \frac{\rho}{\rho_e} dz.$$

Substitution of the velocity profile (11) into the definitions (10) yields

$$H_1 = \frac{2\bar{H}}{\bar{H} - 1} \tag{12}$$

and

$$\bar{H} = 2n + 1,$$

so that we may write the streamwise velocity profile as

$$\frac{U}{u_e}\left(\frac{Z}{Z_\delta}\right)^{\bar{H}-1/2}. \tag{13}$$

3.2. Crossflow Velocity Profiles

For incompressible flow Mager[3] has proposed the relationship

$$\frac{V}{U} = \left(1 - \frac{z}{\delta}\right)^2 \tan(\beta),$$

where V is the crossflow velocity, U is the streamwise velocity and β is the angle between the external streamline and the corresponding limiting streamline on the surface of the body. For compressible flow we assume that the Mager profile may be generalised as

$$\frac{V}{U} = \left(1 - \frac{Z}{Z_\delta}\right)^2 \tan(\beta). \tag{14}$$

As noted in Ref. 2, experimental support for the introduction of the correlating variable Z/Z_δ in equation (14) consists solely of the observation by Hall and Dickens[4] that such a change of variable made an already poor agreement between measured and predicted velocity profiles no worse.

With the assumption of the velocity profiles (13) and (14), all the crossflow integral thicknesses may be related to the streamwise momentum thickness θ_{11} by relations of the form

$$\begin{aligned}\theta_{21} &= \theta_{11}\tan(\beta)\bar{f}_{21}(\bar{H}),\\ \theta_{12} &= \theta_{11}\tan(\beta)\bar{f}_{12}(\bar{H}),\\ \delta_2 &= \theta_{11}\tan(\beta)\bar{f}_2(\bar{H})\end{aligned} \tag{15}$$

and

$$\theta_{22} = \theta_{11}\tan(\beta)\bar{f}_{22}(\bar{H}).$$

The $\bar{f}$ functions are listed in Appendix C and are identical to those derived by the present author[5] as functions of H for incompressible flow.

An alternative crossflow velocity profile is that suggested for incompressible flow by Johnston,[6] for which in a thin layer adjacent to the wall

$$\frac{V}{U} = \tan(\beta) \tag{16}$$

and over the rest of the boundary layer

$$\frac{V}{u_e} = A\left(1 - \frac{U}{u_e}\right). \tag{17}$$

We assume that equations (16) and (17) apply unchanged to compressible flow and that, as demonstrated by Johnston, we need only consider the relation (17) when evaluating the crossflow integral thicknesses. Using equations (17) and (13) we then derive the relationships

$$\begin{aligned}\theta_{12} &= \theta_{11}A\bar{\bar{f}}_{12}(\bar{H}),\\ \theta_{21} &= \theta_{11}A\bar{\bar{f}}_{21}(\bar{H}),\\ \theta_{22} &= \theta_{11}A^2\bar{\bar{f}}_{22}(\bar{H})\end{aligned} \tag{18}$$

and

$$\delta_2 = \theta_{11} A \bar{\bar{f}}_2(\bar{H})$$

where once more the $\bar{\bar{f}}$ functions are defined in Appendix C.

It will be noted that the relations (15) and (18) have a common form

$$\begin{aligned} \theta_{12} &= \theta_{11} \tan(\gamma) f_{12}(\bar{H}), \\ \theta_{21} &= \theta_{11} \tan(\gamma) f_{21}(\bar{H}), \\ \theta_{22} &= \theta_{11} \tan^2(\gamma) f_{22}(\bar{H}) \end{aligned} \tag{19}$$

and

$$\delta_2 = \theta_{11} \tan(\gamma) f_2(\bar{H}),$$

where for Mager profiles $\gamma = \beta$ and for Johnston profiles $\tan(\gamma) \equiv A$. For the latter profiles we require a relation between A and β and this is derived in Appendix D and takes the form

$$\tan(\beta) = A\left[\frac{0{\cdot}1}{[C_f \cos(\beta)(1 + 0{\cdot}18M^2)]^{\frac{1}{2}}} - 1\right], \tag{20}$$

where C_f is the skin-friction coefficient in the external flow direction.

3.3. Skin-Friction Coefficients

Myring has shown that the two components C_{f1} and C_{f2} along the x- and y-axes may be written in terms of C_f and β as

$$C_{f1} = C_f\left\{\frac{\sin(\lambda - \alpha) - \cos(\lambda - \alpha)\tan(\beta)}{\sin\lambda}\right\}$$

and

$$C_{f2} = C_f\left\{\frac{\sin(\alpha) + \cos(\alpha)\tan(\beta)}{\sin\lambda}\right\}. \tag{21}$$

In the context of the present method, the skin-friction coefficient C_f may be evaluated by any expression which yields C_f in terms of θ_{11}, $\bar{H}$ and the external flow conditions. Here we use the Ludwieg–Tillmann relation modified for compressible flow according to Eckert's reference temperature concept.[7] This relationship is

$$C_f = 0{\cdot}264\left(\frac{\rho_e u_e \theta_{11}}{\mu^*}\right)^{-0{\cdot}268}\left(\frac{T_e}{T^*}\right)10^{-0{\cdot}678\bar{H}}, \tag{22}$$

where $T^*/T_e = 1 + 0{\cdot}13M^2$ for adiabatic flow in air and the viscosity μ^* is evaluated at the temperature T^* by using the power law relationship

$$\left(\frac{\mu^*}{\mu_e}\right) = \left(\frac{T^*}{T_e}\right)^{0{\cdot}89}. \tag{23}$$

The power 0·89 in equation (23) is valid for air at temperatures in the range 90 K $\leqslant T \leqslant$ 300 K.

3.4. The Relationship between H and $\bar{H}$

Spence[8] has shown that the assumption, for adiabatic flow, of a quadratic temperature distribution through the boundary layer, produces the relationship

$$H + 1 = (\bar{H} + 1)(1 + 0{\cdot}2rM^2)$$

where r denotes the recovery factor. Green[9] has suggested that in the evaluation of the shape factor H, the recovery factor is best taken as unity, since over the major portion of the boundary layer the total temperature is constant. We therefore use

$$H + 1 = (\bar{H} + 1)(1 + 0{\cdot}2M^2). \tag{24}$$

3.5. The Entrainment Coefficient

For two-dimensional incompressible flow, Head[10] postulated that the entrainment coefficient F is a unique function of the shape parameter H_1, and further, that H_1 is itself a unique function of H. Green has shown that we may combine these two assumptions and write F as a function of H as follows

$$F = 0{\cdot}025H - 0{\cdot}022.$$

Green further suggests that for compressible flow the transformed shape parameter $\bar{H}$ may be taken as the equivalent of the conventional shape parameter in incompressible flow. We now assume that an identical relationship between F and the shape parameter $\bar{H}$ holds in both two- and three-dimensional flows so that we may write

$$F = 0{\cdot}025\bar{H} - 0{\cdot}022. \tag{25}$$

3.6. Final Form of the Equations

Using the trigonometric relationships contained in Appendix B and the empirical relationships of the previous section, we may write equations (2), (3) and (5) in the form

$$\begin{aligned} F_{11}\frac{\partial\theta_{11}}{\partial x} + \theta_{11}F_{11\bar{H}}\frac{\partial\bar{H}}{\partial x} + \theta_{11}F_{11\gamma}\frac{\partial\gamma}{\partial x} &= S_1, \\ F_{21}\frac{\partial\theta_{11}}{\partial x} + \theta_{11}F_{21\bar{H}}\frac{\partial\bar{H}}{\partial x} + \theta_{11}F_{21\gamma}\frac{\partial\gamma}{\partial x} &= S_2 \\ \text{and}\quad J_1\frac{\partial\theta_{11}}{\partial x} + \theta_{11}J_{1\bar{H}}\frac{\partial\bar{H}}{\partial x} + \theta_{11}J_{1\gamma}\frac{\partial\gamma}{\partial x} &= S_3 \end{aligned} \tag{26}$$

where the F's, J's and S's are defined in Appendix E. It should be noted that the x direction has been chosen as the direction of forward integration and that the y derivatives, which will be approximated by finite difference expressions, have been included in the S functions.

When using Mager profiles $\gamma \equiv \beta$ but for Johnston profiles we find, as shown in Appendix D, that we may write γ explicitly in terms of β but not *vice versa*. For both forms of profile we therefore work in terms of β rather than γ and by the method of determinants (Cramer's rule) may rewrite equations (26) in the form

$$\begin{aligned} \frac{\partial\theta_{11}}{\partial x} &= g_1\left(\theta_{11}, \bar{H}, \beta, \frac{\partial\theta_{11}}{\partial y}, \frac{\partial\bar{H}}{\partial y}, \frac{\partial\beta}{\partial y}, u_1, v_1, \frac{\partial u_1}{\partial x}, \frac{\partial u_1}{\partial y}, \frac{\partial v_1}{\partial x}, \frac{\partial v_1}{\partial y}, h_1, h_2, g, \frac{\partial h_1}{\partial x}, \frac{\partial h_1}{\partial y}, \frac{\partial h_2}{\partial x}, \frac{\partial h_2}{\partial y}, \frac{\partial g}{\partial x}, \frac{\partial g}{\partial y}\right), \\ \frac{\partial\bar{H}}{\partial x} &= g_2(\theta_{11}\text{ etc.}) \\ \text{and}\quad \frac{\partial\beta}{\partial x} &= g_3(\theta_{11}\text{ etc.}). \end{aligned} \tag{27}$$

For computational convenience we introduce a reference Reynolds number $R_\infty \equiv U_\infty c/\nu_\infty$, where U_∞ is a reference velocity, c a reference length and ν_∞ a reference kinematic viscosity. We may then non-dimensionalise all lengths (θ_{11}, h_1, h_2 and $g^{\frac{1}{2}}$) with respect to c and velocities (u_1 and v_1) with respect to U_∞. The form of the equations remains unchanged. Given appropriate initial and boundary conditions these equations may be solved by the numerical method of the next section provided the metric coefficients (h_1, h_2 and g) and the external velocity components u_1 and v_1 are known as functions of x and y. In many cases the metric coefficients may be specified analytically as functions of x and y, but in cases where this is not so a numerical method has been devised to obtain these functions from the Cartesian coordinates of the surface coordinate system. Full details are given in Ref. 11 and for completeness the method is outlined here in Appendix F. A method has

The use of these equations implies that if fluid is entering the computational region through either of the side boundaries then boundary conditions must be supplied along that boundary. In some cases this is not possible and the calculation is allowed to proceed by using, for example, a forward difference at the lower boundary if the boundary conditions have not been supplied there. This will have the effect of allowing errors to be propagated into the computational region but the spread of these will be confined to the zone of influence of the first point at which an incorrect difference expression is used.

5. The External Velocity Field

The solution of equations (27) requires that the external velocity distribution be known. Often, however, only a pressure distribution is available and so here a method for deriving the velocity distribution from this pressure distribution is described.

When deriving the momentum integral equations, the pressure p was eliminated by the use of the forms taken by the boundary-layer equations at the outer edge of the layer:

$$\rho_e\left\{\frac{u_1}{h_1}\frac{\partial u_1}{\partial x} + \frac{v_1}{h_2}\frac{\partial u_1}{\partial u} + u_1^2 k_1 + v_1^2 k_2 + u_1 v_1 k_3\right\} = a_1\frac{\partial p}{\partial x} + a_2\frac{\partial p}{\partial y} \tag{33}$$

and

$$\rho_e\left\{\frac{u_1}{h_1}\frac{\partial v_1}{\partial x} + \frac{v_1}{h_2}\frac{\partial v_1}{\partial y} + u_1^2 l_1 + v_1^2 l_2 + u_1 v_1 l_3\right\} = b_1\frac{\partial p}{\partial x} + b_2\frac{\partial p}{\partial y}, \tag{34}$$

where ρ_e is the density at the edge of the boundary layer and the coefficients $k_1, k_2, k_3, l_1, l_2, l_3, a_1, a_2, b_1$ and b_2 are given in Appendix A. We introduce the pressure coefficient C_p defined as

$$C_p = \frac{p - p_\infty}{\frac{1}{2}\rho_\infty U_\infty^2}$$

and at the same time non-dimensionalise all velocities with respect to U_∞. Equations (33) and (34) may then be written as

$$\frac{u_1}{h_1}\frac{\partial u_1}{\partial x} = \frac{1}{2}\frac{\rho_\infty}{\rho_e}\left(a_1\frac{\partial C_p}{\partial x} + a_2\frac{\partial C_p}{\partial y}\right) - u_1^2 k_1 - v_1^2 k_2 - u_1 v_1 k_3 - \frac{v_1}{h_2}\frac{\partial u_1}{\partial y} \tag{35}$$

and

$$\frac{u_1}{h_1}\frac{\partial v_1}{\partial x} = \frac{1}{2}\frac{\rho_\infty}{\rho_e}\left(b_1\frac{\partial C_p}{\partial x} + b_2\frac{\partial C_p}{\partial y}\right) - u_1^2 l_1 - v_1^2 l_2 - u_1 v_1 l_3 - \frac{v_1}{h_2}\frac{\partial v_1}{\partial y} \tag{36}$$

where

$$\frac{\rho_\infty}{\rho_e} = \left(\frac{1 + 0{\cdot}2M^2}{1 + 0{\cdot}2M_\infty^2}\right)^{2\cdot 5} \tag{37}$$

and

$$M = \frac{u_e M_\infty}{[1 + 0{\cdot}2M_\infty^2(1 - u_e^2)]^{\frac{1}{2}}}. \tag{38}$$

Equations (35) and (36) are solved by a numerical method which is similar to that described in the previous section. In this case there is only one family of characteristics, the external streamlines, and so for the evaluation of the y derivatives a backward difference is used if v_1 is positive or a forward difference is used if v_1 is negative. This solution may be obtained simultaneously with the solution of equations (27) or, of course, it may be obtained independently. Once again boundary conditions must be supplied along any boundary through which fluid enters the computational region.

6. Comparisons with Experiments

6.1. Johnston's Impinging Jet Experiment

Johnston[6] measured the boundary-layer development in incompressible flow on the roof of a test section in which a pressure distribution was produced by a jet impinging against the back wall of the test section. A sketch of the test section is given in Fig. 3 where the measuring stations are indicated by small circles. Unfortunately the pressure distribution was not measured in sufficient detail in this experiment and so for the purposes of calculation the external velocity field was assumed to be given by the potential flow solution for an impinging jet. Comparison between the experimental results and calculations using both Mager and Johnston velocity profiles are presented in Figs. 4, 5 and 6. A Cartesian coordinate system was used for these calculations and the integration started 45 inches from the back wall. On the plane of symmetry the agreement between experiment and calculation is excellent until very close to separation. Off the centre line comparison is rendered difficult by the asymmetry which is present in the experimental results. The calculated results remain symmetric because, as is mentioned above, a symmetric pressure distribution was used in the calculations.

Pierce and Klinksiek[12] have recently presented a solution for this flow using streamline coordinates, momentum integral and entrainment equations and Mager profiles. Compared to the results of the present method, Pierce and Klinksiek's results for streamwise momentum thickness are in slightly worse agreement with experiment. Their results for shape factor are in significantly worse agreement, whilst predictions for the limiting streamline angle are about the same. The numerical method used by Pierce and Klinksiek appears to take no account of the hyperbolic nature of the equations used, and it is felt that it is this rather than the slightly different empirical relationships used in their method, which results in their failure to obtain such good agreement with experiment.

6.2. Vermeulen's Curved Duct Experiments

Vermeulen[13] measured the incompressible boundary-layer development on the roof of a 60 degree curved duct. Two sets of measurements were made, the first denoted as Series 1, had no pressure rise between duct inlet and outlet whilst in the Series 2 measurements a pressure rise was produced by introducing a baffle at the duct exit and venting the duct sidewalls. Fig. 7 shows a sketch of the Series 1 measuring positions together with the external and limiting streamlines deduced from the measurements by Vermeulen. Calculations were performed over a grid through the measuring stations. It will be seen from Fig. 7 that boundary-layer fluid is entering the computational region across the line through the measuring stations on the outside of the bend and so the measured boundary conditions for θ_{11}, $\bar{H}$ and β were imposed along this line.

A feature of the coordinate system used in these calculations is the existence of discontinuities in the metric coefficient h_1 at the junctions between straight and curved portions of the duct. To investigate what effect this had upon the results two calculations were performed. In the first the metric coefficients were evaluated by the method described in Appendix F so that the discontinuity was numerically 'smoothed over'. In the second calculation the metric coefficients were used in their discontinuous form. No significant differences were detected between the results of the two calculations.

Figs. 8 to 16 show comparisons between the measurements and calculations using both the Mager and Johnston crossflow models. It will be seen that the predictions for streamwise thickness depart fairly markedly from the measured values but that the streamwise shape factor and the limiting streamline angle are in much better agreement with experiment. The limiting streamline angle is better predicted by the use of the Mager rather than the Johnston crossflow model. The explanation for this discrepancy between experiment and calculation is not at present resolved. One possible explanation is that the crossflow velocity profiles used are not adequate for this case in which the dominant term in the streamwise momentum integral equation is the rate of change in the crosswise direction of the crosswise momentum thickness θ_{12}. Against this explanation we must set the results of calculations for this experiment by Wesseling which were presented at the recent Euromech Colloquium No. 33 on three-dimensional turbulent boundary layers. Wesseling made calculations using his[14] three-dimensional version of Bradshaw's finite difference calculation method so that no velocity profile assumptions were involved. Wesseling's predictions also deviated significantly from the data and appeared to be in closer agreement with the present calculations.

The result of calculations for the Series 2 measurements is shown in Figs. 17 to 26. As with the Series 1 measurements the calculated streamwise momentum thickness does not agree with the measurements but the shape factor and limiting streamline angle are fairly well predicted over most of the length of the duct.

6.3. East's Half Delta Experiment

A sketch of the model used by East[15] is shown in Fig. 27. The tests were made at a velocity of 60 m/s and an incidence of approximately 11 degrees. Boundary-layer measurements were made at twenty-one points along a line inclined at 8 degrees to the vertical which intersected the tunnel floor at a distance of 5·53 m from the apex of the wing. The location of these measurements is shown as traverse position B in the figure. Measurements were also made 0·25 m upstream and downstream of this position to enable gradients of boundary layer and freestream quantities in the chordwise direction to be determined. These measurements indicated that the freestream flow approximated closely to conic conditions (i.e. variations along rays through the apex were small) whilst the streamwise momentum integral thickness appeared to vary almost linearly with distance from the apex. Calculations were therefore made, using polar coordinates, from a position 2 m upstream of the measuring station with starting values as follows—the streamwise momentum thickness was taken to be that at the measuring station scaled by the factor 3·53/5·53, the streamwise shape factor and limiting streamline angle were taken to be the measured values. No side boundary conditions were imposed since the lower boundary was assumed to be a plane of symmetry and fluid was leaving the computational region over the entire length of the upper boundary. Figs. 28 and 29 show the results of these calculations and it will be seen that the momentum thickness is very well predicted, the shape factor is well predicted and once again the use of Mager profiles gives better prediction of the limiting streamline angle than does the use of the Johnson profile.

A feature of this flow is that the domain of dependence becomes progressively narrower as one moves upstream. A result of this is that the flow at the measuring station becomes less and less dependent upon the starting conditions the further upstream the calculation is started. To illustrate this feature calculations were also made starting both 3 and 4 m upstream of the measuring station with the same starting conditions as were used 2 m upstream (i.e. θ_{11} scaled by 3·53/5·53, and not by 2·53/5·53 or 1·53/5·53). The results of these calculations only differed near the wing root and were identical in the region covered by the measurements.

6.4 The Infinite Swept Wing of van den Berg and Elsenaar[16]

In this experiment considerable care was exercised in an attempt to simulate infinite swept wing conditions in incompressible flow. The test surface was a flat plate swept at 35 degrees and a pressure distribution was imposed upon this by a body also swept at 35 degrees. Boundary-layer measurements were made at the position shown in Fig. 30 and also at four other positions along the starting line of the calculation. These latter measurements confirmed that the boundary-layer quantities were invariant along the starting line. Two types of calculation have been performed for this case. In one the pressure distribution as measured over the calculation region was used and in the other infinite swept-wing conditions were assumed and the pressure distribution at all spanwise stations was taken to be that at the measurement plane. In both cases a coordinate system skewed at 35 degrees was used.

No boundary conditions were needed along the line denoted by H in Fig. 30 since fluid was leaving the computational region over the whole length of this line. Along the line C boundary conditions should have been imposed. None were in fact available but the region of influence of the errors introduced by this does not cross the measurement plane until the separation line is reached. Experimentally separation was observed to occur between stations 8 and 9. The comparison between experiment and calculation for streamwise momentum thickness given in Fig. 31 shows that both types of calculation agree well with experiment up to station 6 after which the fully three-dimensional calculation lies a little closer to the experimental points than does the infinite yawed wing calculation. Some of the discrepancy between calculation and experiment may be due to the small static pressure variation through the layer downstream of station 7 which was observed experimentally. It will be seen that the fully three-dimensional calculation using Johnston profiles gives the better agreement with experiment in this case. The above remarks apply equally well to the comparison between measured and calculated streamwise shape factor development shown in Fig. 32. For both streamwise momentum thickness and shape factor the significant differences between experiment and calculation all occur within a distance of about five boundary-layer thicknesses from separation. The predictions for the limiting streamline angle are shown in Fig. 33 and it will be seen that the use of Johnston profiles tends to overestimate the limiting streamline angle whilst the converse is true for the use of Mager profiles. As a result of this the method predicts separation between stations 7 and 8 with Johnston profiles and does not predict separation with Mager profiles. As noted above, experimentally separation was observed between stations 8 and 9.

6.5. The Supersonic Nozzle of Hall and Dickens[4]

Hall and Dickens measured the boundary-layer development on the insulated side wall of a specially constructed supersonic nozzle. The measurements were made along three streamlines denoted by A, B and C in Fig. 34 which also shows the nozzle geometry and the Mach number distribution along streamline B. For the purposes of calculation a coordinate system consisting of the streamlines and lines of x = const was used. Here x denotes distance along the nozzle axis. Using the measured conditions along lines A and C as boundary conditions the results shown in Figs. 35 and 36 were obtained along streamline B. It will be seen that the momentum thickness is well predicted but that the shape factor predictions are consistently below the experimental values. This discrepancy is thought to have been caused by the favourable pressure gradient which existed over the initial portion of the nozzle. The entrainment method in two dimensions performs less well in favourable pressure gradients. To check this a further calculation was made starting at $x = 15$ inches and the results are shown in Figs. 37 and 38. It will be seen that the momentum thickness predictions are still very good whilst the shape factor and limiting streamline angle predictions have improved. The crossflows in this experiment are small and as a result of this the zones of influence of the boundaries A and C do not cross the streamline B. To confirm that this property was also demonstrated by the numerical solutions, calculations were performed in which boundary conditions were not assumed along lines A and C. The results of these calculations gave results identical to those in Figs. 37 and 38.

Shanebrook and Sumner[17] have recently presented the results of calculations using the momentum integral and entrainment equation together with the small crossflow assumption for this flow. The results for streamwise momentum thickness as predicted by Shanebrook and Sumner are very much worse than predictions obtained using the present method. The method of Ref. 17 gives an error of about 25 per cent in momentum thickness at the end of the test region, presumably because the small crossflow assumption is invalid there. The present method is about 2 per cent in error at this point. Shanebrook and Sumner use a crossflow velocity profile which is specifically designed to allow the crossflow to change sign through the boundary layer (neither the Mager nor Johnston profiles can allow for this) but contrary to expectations this does not appear to offer any improvement in prediction of the limiting streamline angle over that given by the present method for this case, even in those regions where the small crossflow assumption is valid.

6.6. General

With the exception of Vermeulen's curved duct, the comparisons with experiment given here show encouraging agreement with experiment. For those flows in which the crossflow changes sign (East, and Hall and Dickens) the Mager profile appears to give the better predictions for limiting streamline angle. For the other flows the Johnston profile gives slightly the better results.

The computer time required for the calculations varies linearly with the number of steps used in the x and y directions. It is given approximately by

$$T = 0{\cdot}008 N_x N_y \text{ seconds}$$

on a CDC 6600 computer where N_x and N_y are the number of steps in the x and y directions. On an ICL 4130 computer the seconds in the above expression become minutes.

7. Conclusions

The boundary-layer prediction method of Myring which uses the momentum integral and entrainment equations in a general coordinate system has been extended here to compressible adiabatic flow. The numerical method which has been developed for the solution of these equations takes account of their hyperbolic nature in the choice of forward step size, the direction in which crosswise derivatives are evaluated and in the imposition of boundary values. For cases where the metric coefficients of the coordinate system used are not known analytically, a method has been developed for obtaining them approximately from the Cartesian coordinates of the surface. This results in an extremely flexible computer program which enabled all the results contained herein, involving five different coordinate systems, to be obtained with no changes to the program. Comparison with experiment, with the exception of Vermeulen's curved duct, is encouraging both in incompressible and compressible flow. The method requires that the velocity distribution external to the boundary layer be known but in many cases this is not so and only a pressure distribution is available. For these cases a method has been developed for calculating the velocity distribution from the given pressure distribution. This calculation is performed simultaneously with the boundary-layer calculation.

LIST OF SYMBOLS

A	Variable in Johnston's crossflow profile
$a_1, a_2, b_1, b_2,$ $k_1, k_2, k_3,$ l_1, l_2, l_3	Coefficients defined in Appendix A
c	Reference length
C_f	Skin-friction coefficient in external stream direction
C_{f1}	Skin-friction coefficient in x direction
C_{f2}	Skin-friction coefficient in y direction
C_p	Pressure coefficient
F	Entrainment coefficient
F_{11}, J_1 etc.	Coefficients relating integral thickness in different coordinate systems. Defined in Appendix E
f_{12} etc.	Functions defined in Appendix C
h_1, h_2, g	Metric coefficients of x, y coordinate system
$H, H_1, \bar{H}$	Shape factors defined in equation (10)
M	Mach number
m	Source strength
p	Static pressure
q	$\equiv \sqrt{h_1^2 h_2^2 - g^2}$
R	$\equiv U_\infty c/\nu_\infty$ reference Reynolds number
r	Recovery factor
S_1 etc.	Defined in Appendix E
U, V	Velocity components in streamline coordinates
u, v, w	Velocity components along x, y, z respectively
$U_1 \equiv u_e$	Resultant velocity in external flow
u_1, v_1, w_1	Values of u, v, w in external flow
x, y, z	Non-orthogonal curvilinear coordinates x, y in body surface, z normal to body surface
α	Angle between x-axis and external streamline
β	Angle between an external streamline and the corresponding streamline at the wall
γ	$\equiv \beta$ for Mager profiles, $\equiv \tan^{-1} A$ for Johnston profiles boundary-layer thickness
δ	Boundary-layer thickness
δ^*	Boundary-layer displacement thickness
Θ_{11}, Δ_1 etc.	integral thicknesses in x, y coordinates
θ_{11}, δ_1 etc.	Integral thicknesses in streamline coordinates
λ	Angle between x and y coordinate directions $\cos(\lambda) \equiv g/(h_1 h_2)$
μ	Viscosity
ρ	Density
ν	$\equiv \mu/\rho$ kinematic viscosity

REFERENCES

No.	*Author*	*Title, etc.*
1	D. F. Myring	An integral prediction method for three-dimensional turbulent boundary layers in incompressible flow. R.A.E. Technical Report 70147 A.R.C. 32647 (1970).
2	P. D. Smith	A calculation method for the turbulent boundary layer on an infinite yawed wing in compressible, adiabatic flow. R.A.E. Technical Report 72193 A.R.C. 34388 (1972).
3	A. Mager	Generalisation of boundary-layer momentum integral equations to three-dimensional flows, including those of rotating systems. N.A.C.A. Report 1067 (1952).
4	M. G. Hall and H. B. Dickens ..	Measurements in a three-dimensional turbulent boundary layer in supersonic flow. A.R.C. R. & M. 3537 (1966).
5	P. D. Smith	Calculation methods for three-dimensional turbulent boundary layers. A.R.C. R. & M. 3523 (1966).
6	J. P. Johnston	Three-dimensional turbulent boundary layers. M.I.T. Gas Turbine Lab. Report 39 (1957).
7	J. E. Green	The prediction of turbulent boundary layer development in compressible flow. *J. Fluid. Mech.* Vol. 31, pt. 4 (1968).
8	D. A. Spence	The growth of compressible turbulent boundary layers on isothermal and adiabatic walls. A.R.C. R. & M. 3191 (1961).
9.	J. E. Green	Application of Head's entrainment method to the prediction of turbulent boundary layers and wakes in compressible flow. R.A.E. Technical Report 72079 A.R.C. 34052 (1972).
10	M. R. Head	Entrainment in the turbulent boundary layer. A.R.C. R. & M. 3152 (1958).
11	P. D. Smith and P. L. Gaffney ..	Approximation of the surface metric tensor by means of bicubic spline interpolation. R.A.E. Technical Report 72185 A.R.C. 34312 (1972).
12	F. J. Pierce and W. F. Klinksiek ..	A momentum integral solution of a three-dimensional boundary layer. A.S.M.E. Paper 72-FE-1 (1972).
13	A. J. Vermeulen	Measurements of three-dimensional turbulent boundary layers. Ph.D. Thesis, Cambridge University (1971).
14	P. Wesseling and J. P. F. Lindhout	A calculation method for three-dimensional incompressible turbulent boundary layers. AGARD CP 93 pp. 8–1, 8–13 (1971).
15	L. F. East	Measurements of the turbulent boundary layer on a slender wing. Unpublished M.O.D. (P.E.) material.

16 B. van den Berg and A. Elsenaar .. Measurements in a three-dimensional incompressible turbulent boundary layer in an adverse pressure gradient under infinite swept wing conditions.
N.L.R. T.R. 72092 U (1972).

17 J. R. Shanebrook and W. J. Sumner A small crossflow theory for three-dimensional, compressible turbulent boundary layers on adiabatic walls.
A.J.A.A. Journal Vol. 11 No. 7 (1973).

APPENDIX A

Definition of Integral Thicknesses

The integral thicknesses are convenient velocity grouping integrals taken across the thickness of the boundary layer, and here two sets are defined corresponding to the two axis systems under consideration.

For the general non-orthogonal axes x and y, lower case u and v have been used to represent the respective velocities. These will now be associated with upper case symbols which represent the integral thicknesses. As used in equation (5), δ represents the real boundary-layer thickness measured normal to the surface and

$$\Theta_{11} = \int_0^\delta \frac{\rho u}{\rho_e u_e^2}(u_1 - u)\,dz, \tag{A-1}$$

$$\Theta_{12} = \int_0^\delta \frac{\rho v}{\rho_e u_e^2}(u_1 - u)\,dz, \tag{A-2}$$

$$\Theta_{21} = \int_0^\delta \frac{\rho u}{\rho_e u_e^2}(v_1 - v)\,dz, \tag{A-3}$$

$$\Theta_{22} = \int_0^\delta \frac{\rho v}{\rho_e u_e^2}(v_1 - v)\,dz, \tag{A-4}$$

$$\Delta_1 = \int_0^\delta \frac{(\rho_e u_1 - \rho u)}{\rho_e u_e}\,dz, \tag{A-5}$$

$$\Delta_2 = \int_0^\delta \frac{(\rho_e v_1 - \rho v)}{\rho_e u_e}\,dz, \tag{A-6}$$

where subscript 1 denotes conditions just external to the boundary layer and u_e is the resultant external velocity given by

$$u_e^2 = u_1^2 + v_1^2 + 2\cos\lambda u_1 v_1. \tag{A-7}$$

In the more familiar case of streamline coordinates s, n where s is measured along an external streamline and n normal to it, upper case U and V have been used as velocities along s and n. However, since the flow is independent of the axis system, the resultant external velocity must be the same as before and hence by definition

$$u_e = U_1. \tag{A-8}$$

With this system similar integral thicknesses may be defined, using lower case representative symbols, as

$$\theta_{11} = \int_0^\delta \frac{\rho U}{\rho_e u_e^2}(U_1 - U)\,dz, \tag{A-9}$$

$$\theta_{12} = \int_0^\delta \frac{\rho V}{\rho_e u_e^2}(U_1 - U)\,dz, \tag{A-10}$$

$$\theta_{21} = \int_0^\delta -\frac{\rho U V}{\rho_e u_e^2}\,dz, \tag{A-11}$$

$$\theta_{22} = \int_0^\delta -\frac{\rho V^2}{\rho_e u_e^2}\,dz, \tag{A-12}$$

$$\delta_1 = \int_0^\delta \frac{(\rho_e U_1 - \rho U)}{\rho_e u_e^2}\,dz, \tag{A-13}$$

$$\delta_2 = \int_0^{\delta} -\frac{\rho V}{\rho_e u_e}\, dz, \tag{A-14}$$

where U_1 has been retained for comparative purposes.

The quantities k_1, k_2, k_3, l_1, l_2, l_3, a_1, a_2, b_1, b_2 and q which appear in equations (2), (3), (33) and (34) are defined as the following functions of the metric coefficients h_1, h_2 and g:

$$k_1 = \frac{h_1 g}{q^2}\left\{\frac{1}{h_1}\frac{\partial h_1}{\partial y} + \frac{g}{h_1^3}\frac{\partial h_1}{\partial x} - \frac{1}{h_1^2}\frac{\partial g}{\partial x}\right\}, \tag{A-15}$$

$$k_2 = \frac{h_1}{q}\left\{\frac{\partial g}{\partial y} - h_2\frac{\partial h_2}{\partial x} - \frac{g}{h_2}\frac{\partial h_2}{\partial y}\right\}, \tag{A-16}$$

$$k_3 = \frac{1}{q^2}\left\{h_1 h_2\left(1 + \frac{g^2}{h_1^2 h_2^2}\right)\frac{\partial h_1}{\partial y} - 2g\frac{\partial h_2}{\partial x}\right\}, \tag{A-17}$$

$$l_1 = \frac{h_2}{q^2}\left\{\frac{\partial g}{\partial x} - h_1\frac{\partial h_1}{\partial y} - \frac{g}{h_1}\frac{\partial h_1}{\partial x}\right\}, \tag{A-18}$$

$$l_2 = \frac{g h_2}{q^2}\left\{\frac{1}{h_2}\frac{\partial h_2}{\partial x} + \frac{g}{h_2^3}\frac{\partial h_2}{\partial y} - \frac{1}{h_2^2}\frac{\partial g}{\partial y}\right\}, \tag{A-19}$$

$$l_3 = \frac{1}{q^2}\left\{h_1 h_2\left(1 + \frac{g^2}{h_1^2 h_2^2}\right)\frac{\partial h_2}{\partial x} - 2g\frac{\partial h_1}{\partial y}\right\}, \tag{A-20}$$

$$q^2 = h_1^2 h_2^2 - g^2. \tag{A-21}$$

$$a_1 = -\frac{h_2^2 h_1}{q^2}, \tag{A-22}$$

$$a_2 = \frac{g h_1}{q^2}, \tag{A-23}$$

$$b_1 = \frac{g h_2}{q^2} \tag{A-24}$$

and

$$b_2 = -\frac{h_2 h_1^2}{q^2}. \tag{A-25}$$

APPENDIX B

Relationships Between the Integral Thicknesses of the Two Axis Systems

Fig. 1 shows the two axis systems and by resolution

$$u = \frac{U \sin(\lambda - \alpha) - V \cos(\lambda - \alpha)}{\sin \lambda}, \qquad u_1 = U_1 \frac{\sin(\lambda - \alpha)}{\sin \lambda},$$
$$v = \frac{U \sin \alpha + V \cos \alpha}{\sin \lambda}, \qquad v_1 = U_1 \frac{\sin \alpha}{\sin \lambda}. \tag{B-1}$$

Hence

$$\rho_e u_e^2 \Theta_{11} = \int_0^\delta \rho u(u_1 - u)\, dz,$$

$$= \int_0^\delta \rho[U_1 \sin(\lambda - \alpha)\{U \sin(\lambda - \alpha) - V \cos(\lambda - \alpha)\} - U^2 \sin^2(\lambda - \alpha)$$

$$+ 2UV \sin(\lambda - \alpha)\cos(\lambda - \alpha) - V^2 \cos^2(\lambda - \alpha)] \frac{dz}{\sin^2 \lambda},$$

and thus

$$\Theta_{11} = \frac{\theta_{11} \sin^2(\lambda - \alpha) - (\theta_{12} + \theta_{21}) \sin(\lambda - \alpha)\cos(\lambda - \alpha) + \theta_{22} \cos^2(\lambda - \alpha)}{\sin^2 \lambda}. \tag{B-2}$$

Similarly,

$$\rho_e u_e^2 \Theta_{12} = \int_0^\delta \rho v(u_1 - u)\, dz,$$

$$= \int_0^\delta \rho[U_1 \sin(\lambda - \alpha)\{U \sin \alpha + V \cos \alpha\} -$$

$$- U \sin(\lambda - \alpha) - V \cos(\lambda - \alpha)\}\{U \sin \alpha + V \cos \alpha\}] \frac{dz}{\sin^2 \lambda},$$

and hence,

$$\Theta_{12} = \frac{[\theta_{11} \sin \alpha \sin(\lambda - \alpha) + \theta_{12} \sin(\lambda - \alpha) \cos \alpha - \theta_{21} \cos(\lambda - \alpha) \sin \alpha - \theta_{22} \cos \alpha \cos(\lambda - \alpha)]}{\sin^2 \lambda}. \tag{B-3}$$

This process may be repeated for the remaining terms to render

$$\Theta_{21} = \frac{[\theta_{11} \sin \alpha \sin(\lambda - \alpha) + \theta_{21} \sin(\lambda - \alpha) \cos \alpha - \theta_{12} \cos(\lambda - \alpha) \sin \alpha - \theta_{22} \cos \alpha \cos(\lambda - \alpha)]}{\sin^2 \lambda}, \tag{B-4}$$

$$\Theta_{22} = \frac{[\theta_{11} \sin^2 \alpha + (\theta_{12} + \theta_{21}) \cos \alpha \sin \alpha + \theta_{22} \cos^2 \alpha]}{\sin^2 \lambda}, \tag{B-5}$$

$$\Delta_1 = \frac{\delta_1 \sin(\lambda - \alpha) - \delta_2 \cos(\lambda - \alpha)}{\sin \lambda} \tag{B-6}$$

and

$$\Delta_2 = \frac{\delta_1 \sin \alpha + \delta_2 \cos \alpha}{\sin \lambda}. \tag{B-7}$$

It is therefore clear that the integral thicknesses of one axis system are simply related to those of the other, and that one set completely determines the other.

One advantage sometimes claimed for the use of streamline coordinates is that there exists an identity

$$\theta_{12} \equiv \theta_{21} - \delta_2 \tag{B-8}$$

which reduces the number of unknowns. In fact (B-8) is merely a particular form of the general identity

$$\Theta_{12} \equiv \Theta_{21} - \Delta_2 \frac{\sin (\lambda - \alpha)}{\sin \lambda} + \Delta_1 \frac{\sin \alpha}{\sin \lambda}, \tag{B-9}$$

which holds for any coordinate system. The angles λ and α appearing in the above expressions are related to the metric coefficients of the coordinate system and the external flow as follows

$$\cos (\lambda) = \frac{g}{h_1 h_2} \tag{B-10}$$

and

$$\sin (\alpha) = \frac{v_1 \sin \lambda}{u_e}.$$

APPENDIX C

Crossflow Profile Functions

The functions f of equations (15) and (18) are listed in this Appendix. They are formally identical to those given by Myring as functions of H but have been rearranged into a form which is more convenient for computation. For Mager profiles:

$$\begin{aligned}
\bar{f}_{21} &= -\frac{2}{(\bar{H}-1)(\bar{H}+2)},\\
\bar{f}_{2} &= -\frac{16\bar{H}}{(\bar{H}-1)(\bar{H}+3)(\bar{H}+5)},\\
\bar{f}_{12} &= \bar{f}_{21} - \bar{f}_{2},\\
\bar{f}_{22} &= \frac{12\bar{f}_{21}}{(\bar{H}+3)(\bar{H}+4)},\\
\bar{f}'_{21} &= \frac{2(2\bar{H}+1)}{(\bar{H}-1)^2(\bar{H}+2)^2},\\
\bar{f}'_{2} &= \frac{\bar{f}_{2}\bar{f}'_{21}}{\bar{f}_{21}} + \frac{48\bar{f}_{21}(\bar{H}^2+5\bar{H}+5)}{(\bar{H}+3)^2(\bar{H}+5)^2},\\
\bar{f}'_{12} &= \bar{f}'_{21} - \bar{f}'_{2}
\end{aligned} \tag{C-1}$$

and

$$\bar{f}'_{22} = \frac{12\bar{f}'_{21} - \bar{f}_{22}(2\bar{H}+7)}{(\bar{H}+3)(\bar{H}+4)}.$$

For Johnston profiles:

$$\begin{aligned}
\bar{\bar{f}}_{21} &= -1,\\
\bar{\bar{f}}_{12} &= \bar{H} - 1,\\
\bar{\bar{f}}_{2} &= -\bar{H},\\
\bar{\bar{f}}_{22} &= -\bar{\bar{f}}_{12},\\
\bar{\bar{f}}'_{21} &= 0,\\
\bar{\bar{f}}'_{12} &= 1,\\
\bar{\bar{f}}'_{2} &= -1,
\end{aligned} \tag{C-2}$$

and

$$\bar{\bar{f}}'_{22} = -1,$$

where the dashes denote differentiation with respect to $\bar{H}$.

APPENDIX D

The Relationship between β and γ for the Johnston Profile

The Johnston profile as given by equations (16) and (17) is, near the wall

$$\frac{V}{U} = \tan(\beta) \tag{D-1}$$

while over the rest of the boundary layer

$$\frac{V}{u_e} = A\left(1 - \frac{U}{u_e}\right). \tag{D-2}$$

Johnston postulated that the matching point for equations (D-1) and (D-2) occurred at a constant value of U_T/U_τ and chose this value to be $10\sqrt{2}$. Here U_T denotes the resultant velocity in the boundary layer, i.e. ($[U^2 + V^2]^{\frac{1}{2}}$) and U_τ is the friction velocity.

Assuming that we may make use of this in compressible flow provided U_τ is based on the density at the wall, we have at the matching point

$$\frac{U_T}{u_e} = 10\sqrt{2}\frac{U_\tau}{u_e} = 10\sqrt{\frac{T_w}{T_e}\frac{C_f}{\cos(\beta)}} \tag{D-3}$$

but $U_T = U\sec(\beta)$ and so (D-3) may be written as

$$\frac{U}{u_e} = 10\sqrt{\frac{T_w}{T_e}C_f\cos(\beta)}. \tag{D-4}$$

At the matching point we may equate (D-1) and (D-2) to yield

$$\tan(\beta) = A\left[\frac{u_e}{U} - 1\right] \tag{D-5}$$

and substituting equation (D-4) into (D-5) gives

$$\tan(\beta) = A\left[\frac{0{\cdot}1}{\sqrt{C_f\frac{T_w}{T_e}\cos(\beta)}} - 1\right]. \tag{D-6}$$

Taking the recovery factor to be equal to 0·9 so that $T_w/T_e = 1 + 0{\cdot}18M^2$ and writing $\tan(\gamma) \equiv A$ we may express γ explicitly in terms of β as

$$\tan(\gamma) = \tan(\beta)\frac{\sqrt{C_f\cos(\beta)(1 + 0{\cdot}18M^2)}}{0{\cdot}10 - \sqrt{C_f\cos(\beta)(1 + 0{\cdot}18M^2)}}. \tag{D-7}$$

APPENDIX E

Reduced Forms of Integral Thicknesses

The coefficients of equations (26) may be assembled from equations (B-2) to (C-2). The complete list of required functions is now readily shown to be:
defining

$$t = \tan \gamma, \tag{E-1}$$

$$F_{11} = [\sin^2(\lambda - \alpha) - (f_{12} + f_{21}) \sin(\lambda - \alpha) \cos(\lambda - \alpha)t + f_{22} \cos^2(\lambda - \alpha)t^2]/\sin^2 \lambda,$$

$$F_{12} = [\sin \alpha \sin(\lambda - \alpha) + \{f_{12} \cos \alpha \sin(\lambda - \alpha) - f_{21} \sin \alpha \cos(\lambda - \alpha)\}t - f_{22} \cos \alpha \cos(\lambda - \alpha)t^2]/\sin^2 \lambda,$$

$$F_{21} = [\sin \alpha \sin(\lambda - \alpha) + \{f_{21} \cos \alpha \sin(\lambda - \alpha) - f_{12} \sin \alpha \cos(\lambda - \alpha)\}t - f_{22} \cos \alpha \cos(\lambda - \alpha)t^2]/\sin^2 \lambda,$$

$$F_{22} = [\sin^2 \alpha + (f_{12} + f_{21}) \sin \alpha \cos \alpha t + f_{22} \cos^2 \alpha t^2]/\sin^2 \lambda,$$

$$F_1 = [H \sin(\lambda - \alpha) - f_2 \cos(\lambda - \alpha)t]/\sin \lambda,$$

$$F_2 = [H \sin \alpha + f_2 \cos \alpha t]/\sin \lambda,$$

$$J_1 = [H_1 \sin(\lambda - \alpha) + f_2 \cos(\lambda - \alpha)t]/\sin \lambda,$$

$$J_2 = [H_1 \sin \alpha - f_2 \cos \alpha t]/\sin \lambda,$$

$$F_{11\bar{H}} = [-(f'_{12} + f'_{21}) \sin(\lambda - \alpha) \cos(\lambda - \alpha)t + f'_{22} \cos^2(\lambda - \alpha)t^2]/\sin^2 \lambda,$$

$$F_{12\bar{H}} = [\{f'_{12} \cos \alpha \sin(\lambda - \alpha) - f'_{21} \sin \alpha \cos(\lambda - \alpha)\}t - f'_{22} \cos \alpha \cos(\lambda - \alpha)t^2]/\sin \lambda,$$

$$F_{21\bar{H}} = [\{f'_{21} \cos \alpha \sin(\lambda - \alpha) - f'_{12} \sin \alpha \cos(\lambda - \alpha)\}t - f'_{22} \cos \alpha \cos(\lambda - \alpha)t^2]/\sin^2 \lambda,$$

$$F_{22\bar{H}} = [(f'_{12} + f'_{21}) \sin \alpha \cos \alpha t + f'_{22} \cos^2 \alpha t^2]/\sin^2 \lambda,$$

$$F_{1\bar{H}} = [(1 + 0{\cdot}2M^2) \sin(\lambda - \alpha) - f'_2 \cos(\lambda - \alpha)t]/\sin \lambda,$$

$$F_{2\bar{H}} = [(1 + 0{\cdot}2M^2) \sin \alpha + f'_2 \cos \alpha t]/\sin \lambda,$$

$$J_{1\bar{H}} = [H'_1 \sin(\lambda - \alpha) + f'_2 \cos(\lambda - \alpha)t]/\sin \lambda,$$

$$J_{2\bar{H}} = [H'_1 \sin \alpha - f'_2 \cos \alpha t]/\sin \lambda,$$

$$F_{11\alpha} = [2 \cos(\lambda - \alpha) \sin(\lambda - \alpha)\{f_{22}t^2 - 1\} + \{f_{12} + f_{21})(2 \cos^2(\lambda - \alpha) - 1)t]/\sin^2 \lambda,$$

$$F_{12\alpha} = [\{\cos \alpha \sin(\lambda - \alpha) - \cos(\lambda - \alpha) \sin \alpha\}\{1 - f_{22}t^2\} - (f_{12} + f_{21})\{\cos \alpha \cos(\lambda - \alpha) +$$

$$+ \sin \alpha \sin(\lambda - \alpha)\}t]/\sin^2 \lambda,$$

$$F_{21\alpha} = F_{11\alpha},$$

$$F_{22\alpha} = [2 \sin \alpha \cos \alpha(1 - f_{22}t^2) + (f_{12} + {}_{21})(2 \cos^2\alpha - 1)t]/\sin^2\lambda,$$

$$F_{1\alpha} = -[H \cos(\lambda - \alpha) + f_2 \sin(\lambda - \alpha)t]/\sin \lambda,$$

$$F_{2\alpha} = [H \cos \alpha - f_2 \sin \alpha t]/\sin \lambda,$$

$$J_{1\alpha} = [-H_1 \cos(\lambda - \alpha) + f_2 \sin(\lambda - \alpha)t]/\sin \lambda,$$

$$J_{2\alpha} = [H_1 \cos\alpha + f_2 \sin\alpha t]/\sin\lambda,$$

$$F_{11\gamma} = [-(f_{12} + f_{21})\sin(\lambda - \alpha)\cos(\lambda - \alpha) + 2f_{22}\cos^2(\lambda - \alpha)t]\frac{(1 + t^2)}{\sin^2\lambda},$$

$$F_{12\gamma} = [f_{12}\sin(\lambda - \alpha)\cos\alpha - f_{21}\cos(\lambda - \alpha)\sin\alpha - 2f_{22}\cos\alpha\cos(\lambda - \alpha)t]\frac{(1 + t^2)}{\sin^2\lambda},$$

$$F_{21\gamma} = [f_{21}\sin(\lambda - \alpha)\cos\alpha - f_{12}\cos(\lambda - \alpha)\sin\alpha - 2f_{22}\cos\alpha\cos(\lambda - \alpha)t]\frac{(1 + t^2)}{\sin^2\lambda},$$

$$F_{22\gamma} = [(f_{12} + f_{21})\sin\alpha\cos\alpha + 2f_{22}\cos^2\alpha t]\frac{(1 + t^2)}{\sin^2\lambda},$$

$$F_{1\gamma} = [-f_2\cos(\lambda - \alpha)]\frac{(1 + t^2)}{\sin\lambda},$$

$$F_{2\gamma} = [f_2\cos\alpha]\frac{(1 + t^2)}{\sin\lambda},$$

$$J_{1\gamma} = -F_{1\gamma},$$

$$J_{2\gamma} = -F_{2\gamma},$$

$$F_{11\lambda} = -[F_{11\alpha} + 2F_{11}\cos\lambda/\sin\lambda],$$

$$F_{12\lambda} = [\cos(\lambda - \alpha)\{\sin\alpha + f_{12}\cos\alpha t\} + \sin(\lambda - \alpha)\{f_{22}\cos\alpha t + f_{21}\sin\alpha\}t - 2F_{12}\sin\lambda\cos\lambda]/\sin^2\lambda,$$

$$F_{21\lambda} = [\cos(\lambda - \alpha)\{\sin\alpha + f_{21}\cos\alpha t\} + \sin(\lambda - \alpha)\{f_{22}\cos\alpha t + f_{12}\sin\alpha\}t - 2F_{21}\sin\lambda\cos\lambda]/\sin^2\lambda,$$

$$F_{22\lambda} = -2F_{22}\cos\lambda/\sin\lambda,$$

$$F_{1\lambda} = [H\cos(\lambda - \alpha) + f_2\sin(\lambda - \alpha)t - F_1\cos\lambda]/\sin\lambda,$$

$$F_{2\lambda} = -F_2\cos\lambda/\sin\lambda,$$

$$J_{1\lambda} = -J_{1\alpha} - J_1\cos\lambda/\sin\lambda \qquad \text{and}$$

$$J_{2\lambda} = -J_2\cos\lambda/\sin\lambda.$$

The S functions contained in equations (26) are given by

$$\begin{aligned} S_1 = \frac{C_{f1}}{2}h_1 - \theta_{11}\Bigg[& F_{11\alpha}\frac{\partial\alpha}{\partial x} + F_{11\lambda}\frac{\partial\lambda}{\partial x} + F_{11}\left(\frac{(2 - M^2)}{u_e}\frac{\partial u_e}{\partial x} + \frac{h_1}{q}\frac{\partial}{\partial x}\left(\frac{q}{h_1}\right) + k_1 h_1\right) + \\ & + \frac{h_1}{h_2}\Bigg(\frac{F_{12}}{\theta_{11}}\frac{\partial\theta_{11}}{\partial y} + F_{12\bar{H}}\frac{\partial\bar{H}}{\partial y} + F_{12\gamma}\frac{\partial\gamma}{\partial y} + F_{12\alpha}\frac{\partial\alpha}{\partial y} + F_{12\lambda}\frac{\partial\lambda}{\partial y} + \\ & + F_{12}\left\{\frac{(2 - M^2)}{u_e}\frac{\partial u_e}{\partial y} + \frac{h_2}{q}\frac{\partial}{\partial y}\left(\frac{q}{h_2}\right) + k_3 h_2\right\}\Bigg) + F_1\left(\frac{1}{u_e}\frac{\partial u_1}{\partial x} + k_1 h_1\frac{u_1}{u_e}\right) + \\ & + F_2\left(\frac{h_1}{h_2}\frac{1}{u_e}\frac{\partial u_1}{\partial y} + k_2 h_1\frac{v_1}{u_e} + k_3 h_1\frac{u_1}{u_e}\right) + F_{22}k_2 h_1\Bigg], \end{aligned} \qquad \text{(E-2)}$$

$$J_{2\alpha} = [H_1 \cos\alpha + f_2 \sin\alpha t]/\sin\lambda,$$

$$F_{11\gamma} = [-(f_{12} + f_{21}) \sin(\lambda - \alpha) \cos(\lambda - \alpha) + 2f_{22} \cos^2(\lambda - \alpha)t]\frac{(1 + t^2)}{\sin^2\lambda},$$

$$F_{12\gamma} = [f_{12} \sin(\lambda - \alpha) \cos\alpha - f_{21} \cos(\lambda - \alpha) \sin\alpha - 2f_{22} \cos\alpha \cos(\lambda - \alpha)t]\frac{(1 + t^2)}{\sin^2\lambda},$$

$$F_{21\gamma} = [f_{21} \sin(\lambda - \alpha) \cos\alpha - f_{12} \cos(\lambda - \alpha) \sin\alpha - 2f_{22} \cos\alpha \cos(\lambda - \alpha)t]\frac{(1 + t^2)}{\sin^2\lambda},$$

$$F_{22\gamma} = [(f_{12} + f_{21}) \sin\alpha \cos\alpha + 2f_{22} \cos^2\alpha t]\frac{(1 + t^2)}{\sin^2\lambda},$$

$$F_{1\gamma} = [-f_2 \cos(\lambda - \alpha)]\frac{(1 + t^2)}{\sin\lambda},$$

$$F_{2\gamma} = [f_2 \cos\alpha]\frac{(1 + t^2)}{\sin\lambda},$$

$$J_{1\gamma} = -F_{1\gamma},$$

$$J_{2\gamma} = -F_{2\gamma},$$

$$F_{11\lambda} = -[F_{11\alpha} + 2F_{11} \cos\lambda/\sin\lambda],$$

$$F_{12\lambda} = [\cos(\lambda - \alpha)\{\sin\alpha + f_{12} \cos\alpha t\} + \sin(\lambda - \alpha)\{f_{22} \cos\alpha t + f_{21} \sin\alpha\}t - 2F_{12} \sin\lambda \cos\lambda]/\sin^2\lambda,$$

$$F_{21\lambda} = [\cos(\lambda - \alpha)\{\sin\alpha + f_{21} \cos\alpha t\} + \sin(\lambda - \alpha)\{f_{22} \cos\alpha t + f_{12} \sin\alpha\}t - 2F_{21} \sin\lambda \cos\lambda]/\sin^2\lambda,$$

$$F_{22\lambda} = -2F_{22} \cos\lambda/\sin\lambda,$$

$$F_{1\lambda} = [H \cos(\lambda - \alpha) + f_2 \sin(\lambda - \alpha)t - F_1 \cos\lambda]/\sin\lambda,$$

$$F_{2\lambda} = -F_2 \cos\lambda/\sin\lambda,$$

$$J_{1\lambda} = -J_{1\alpha} - J_1 \cos\lambda/\sin\lambda \qquad \text{and}$$

$$J_{2\lambda} = -J_2 \cos\lambda/\sin\lambda.$$

The S functions contained in equations (26) are given by

$$\begin{aligned} S_1 = \frac{C_{f1}}{2}h_1 - \theta_{11}\Bigg[& F_{11\alpha}\frac{\partial\alpha}{\partial x} + F_{11\lambda}\frac{\partial\lambda}{\partial x} + F_{11}\left(\frac{(2 - M^2)}{u_e}\frac{\partial u_e}{\partial x} + \frac{h_1}{q}\frac{\partial}{\partial x}\left(\frac{q}{h_1}\right) + k_1 h_1\right) + \\ & + \frac{h_1}{h_2}\left(\frac{F_{12}}{\theta_{11}}\frac{\partial\theta_{11}}{\partial y} + F_{12\bar{H}}\frac{\partial\bar{H}}{\partial y} + F_{12\gamma}\frac{\partial\gamma}{\partial y} + F_{12\alpha}\frac{\partial\alpha}{\partial y} + F_{12\lambda}\frac{\partial\lambda}{\partial y} + \right. \\ & \left. + F_{12}\left\{\frac{(2 - M^2)}{u_e}\frac{\partial u_e}{\partial y} + \frac{h_2}{q}\frac{\partial}{\partial y}\left(\frac{q}{h_2}\right) + k_3 h_2\right\}\right) + F_1\left(\frac{1}{u_e}\frac{\partial u_1}{\partial x} + k_1 h_1\frac{u_1}{u_e}\right) + \\ & + F_2\left(\frac{h_1}{h_2}\frac{1}{u_e}\frac{\partial u_1}{\partial y} + k_2 h_1\frac{v_1}{u_e} + k_3 h_1\frac{u_1}{u_e}\right) + F_{22}k_2 h_1\Bigg], \end{aligned} \qquad \text{(E-2)}$$

$$S_2 = \frac{C_{f2}}{2} h_1 - \theta_{11}\left[F_{21\alpha}\frac{\partial\alpha}{\partial x} + F_{21\lambda}\frac{\partial\lambda}{\partial x} + F_{21}\left(\frac{(2 - M^2)}{u_e}\frac{\partial u_e}{\partial x} + \frac{h_1}{q}\frac{\partial}{\partial x}\left(\frac{q}{h_1}\right) + l_3 h_1\right) + \right.$$

$$+ \frac{h_1}{h_2}\left(\frac{F_{22}}{\theta_{11}}\frac{\partial\theta_{11}}{\partial y} + F_{22\bar{H}}\frac{\partial\bar{H}}{\partial y} + F_{22\gamma}\frac{\partial\gamma}{\partial y} + F_{22\alpha}\frac{\partial\alpha}{\partial y} + F_{22\lambda}\frac{\partial\lambda}{\partial y} + \right.$$

$$\left. + F_{22}\left\{\frac{(2 - M^2)}{u_e}\frac{\partial u_e}{\partial y} + \frac{h_2}{q}\frac{\partial}{\partial y}\left(\frac{q}{h_2}\right) + l_2 h_2\right\}\right) + F_1\left(\frac{1}{u_e}\frac{\partial v_1}{\partial x} + l_1 h_1 \frac{u_1}{u_e} + l_3 h_1 \frac{v_1}{u_e}\right) +$$

$$\left. + F_2\left(\frac{h_1}{h_2}\frac{1}{u_e}\frac{\partial v_1}{\partial y} + l_2 h_1 \frac{v_1}{u_e}\right) + l_1 h_1\right], \tag{E-3}$$

$$S_3 = F h_1 - \theta_{11}\left[J_{1\alpha}\frac{\partial\alpha}{\partial x} + J_{1\lambda}\frac{\partial\lambda}{\partial x} + \frac{h_1}{h_2}\left(\frac{J_2}{\theta_{11}}\frac{\partial\theta_{11}}{\partial y} + J_{2\bar{H}}\frac{\partial\bar{H}}{\partial y} + J_{2\gamma}\frac{\partial\gamma}{\partial y} + J_{2\alpha}\frac{\partial\alpha}{\partial y} + J_{2\lambda}\frac{\partial\lambda}{\partial y}\right) + \right.$$

$$\left. + J_1\left(\frac{h_1}{q}\frac{\partial}{\partial x}\left(\frac{q}{h_1}\right) + \frac{(1 - M^2)}{u_e}\frac{\partial u_e}{\partial x}\right) + \frac{h_1}{h_2} J_2\left(\frac{h_2}{q}\frac{\partial}{\partial y}\left(\frac{q}{h_2}\right) + \frac{(1 - M^2)}{u_e}\frac{\partial u_e}{\partial y}\right)\right]. \tag{E-4}$$

APPENDIX F

Evaluation of the Metric Coefficients of the Surface Coordinate System[11]

We assume that the Cartesian coordinates X, Y, Z of the surface are known and on the surface we have the curvilinear coordinate system x, y such that each point x, y defines a unique point X, Y, Z on the surface. Then there exists a transformation between the two coordinate systems which we may write as

$$\left.\begin{aligned} X &= p_1(x, y), \\ Y &= p_2(x, y), \\ Z &= p_3(x, y), \end{aligned}\right\} \tag{F-1}$$

and the metric coefficients h_1, h_2 and g of the curvilinear coordinate system are given by

$$h_1^2 = \left(\frac{\partial p_1}{\partial x}\right)^2 + \left(\frac{\partial p_2}{\partial x}\right)^2 + \left(\frac{\partial p_3}{\partial x}\right)^2,$$

$$h_2^2 = \left(\frac{\partial p_1}{\partial y}\right)^2 + \left(\frac{\partial p_2}{\partial y}\right)^2 + \left(\frac{\partial p_3}{\partial y}\right)^2 \tag{F-2}$$

and

$$g = \frac{\partial p_1}{\partial x}\frac{\partial p_1}{\partial y} + \frac{\partial p_2}{\partial x}\frac{\partial p_2}{\partial y} + \frac{\partial p_3}{\partial x}\frac{\partial p_3}{\partial y}.$$

Differentiating equations (F-2) with respect to x and y we obtain

$$h_1\frac{\partial h_1}{\partial x} = \frac{\partial p_1}{\partial x}\frac{\partial^2 p_1}{\partial x^2} + \frac{\partial p_2}{\partial x}\frac{\partial^2 p_2}{\partial x^2} + \frac{\partial p_3}{\partial x}\frac{\partial^2 p_3}{\partial x^2}$$

and

$$h_1\frac{\partial h_1}{\partial y} = \frac{\partial p_1}{\partial x}\frac{\partial^2 p_1}{\partial x \partial y} + \frac{\partial p_2}{\partial x}\frac{\partial^2 p_2}{\partial x \partial y} + \frac{\partial p_3}{\partial x}\frac{\partial^2 p_3}{\partial x \partial y} \tag{F-3}$$

with similar expressions for $\partial h_2/\partial x$, $\partial h_2/\partial y$, $\partial g/\partial x$ and $\partial g/\partial y$. In cases in which the functions $p_1 \rightarrow p_3$ are known analytically it is thus simply a matter of algebra to obtain the metric coefficients and their derivatives with respect to x and y. In cases where these functions are not known and must be approximated it will be seen that the above expressions imply that if the metric coefficients are to have continuous derivatives then any approximating functions used for p_1, p_2 and p_3 must have at least continuous second derivatives. The technique we have adopted is described in Ref. 11 and is as follows. We assume that the Cartesian coordinates of the surface are known at the mesh points defined by the intersections of two families of curves x = const and y = const. We then approximate the functions p_1, p_2 and p_3 by three bicubic splines which have continuous second derivatives and agree with the known values at the mesh points. These approximate forms for p_1, p_2 and p_3 are then used in equations (F-2) and (F-3) to calculate the metric coefficients h_1, h_2 and g together with their first derivatives with respect to x and y.

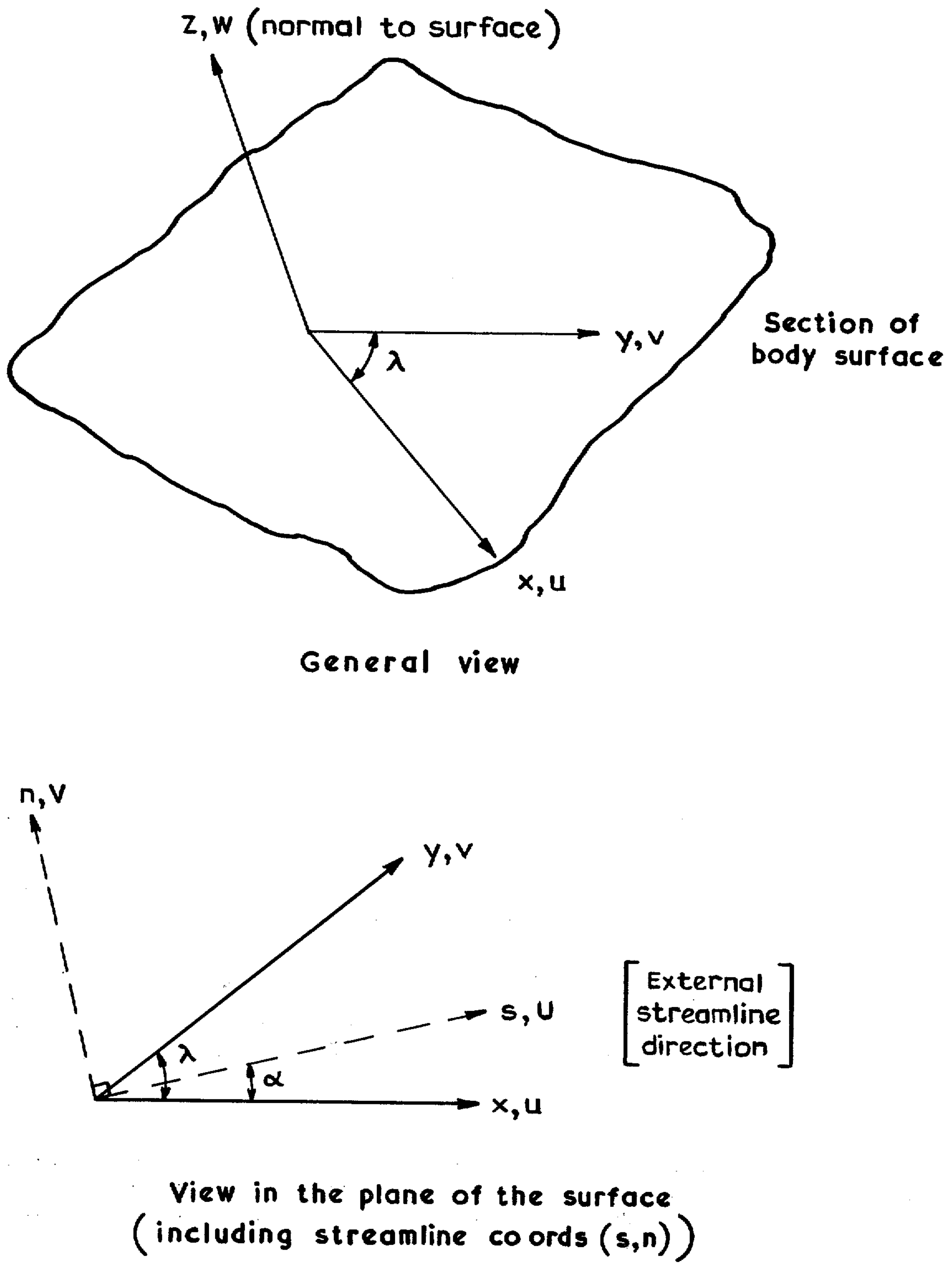

FIG. 1. Coordinate system used.

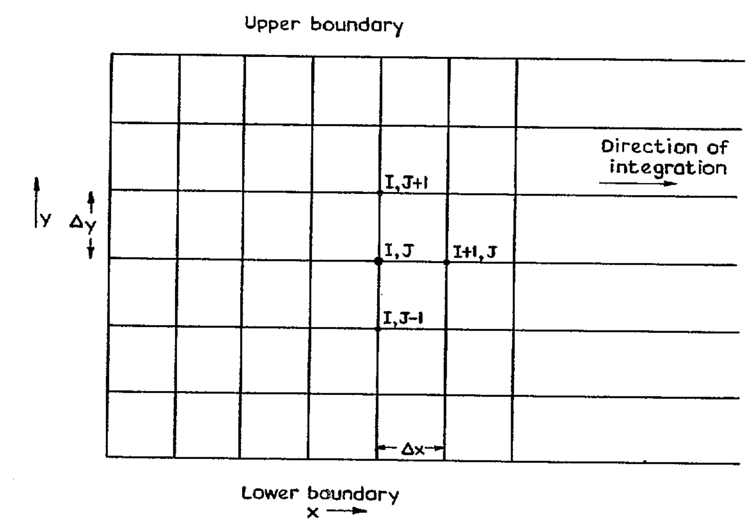

FIG. 2. Computational mesh.

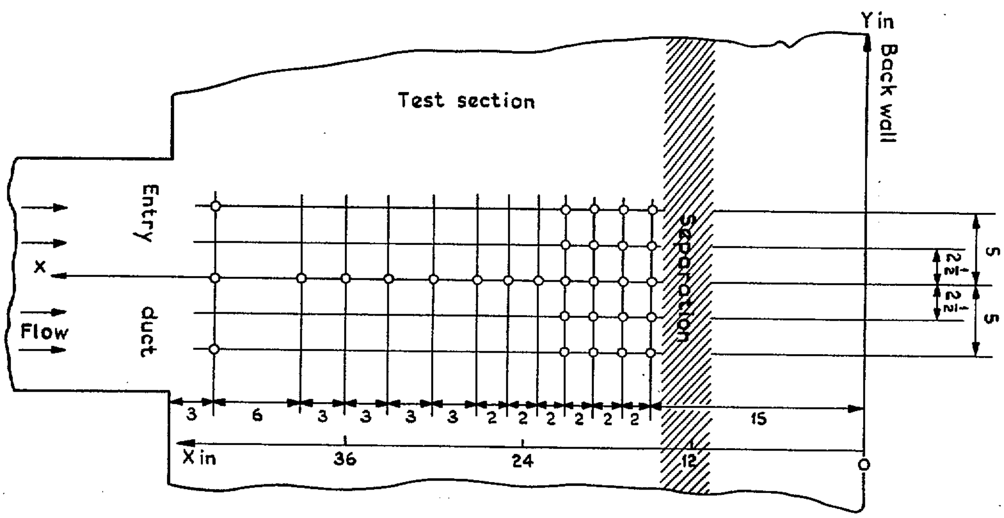

FIG. 3. Johnston's impinging jet experiment.

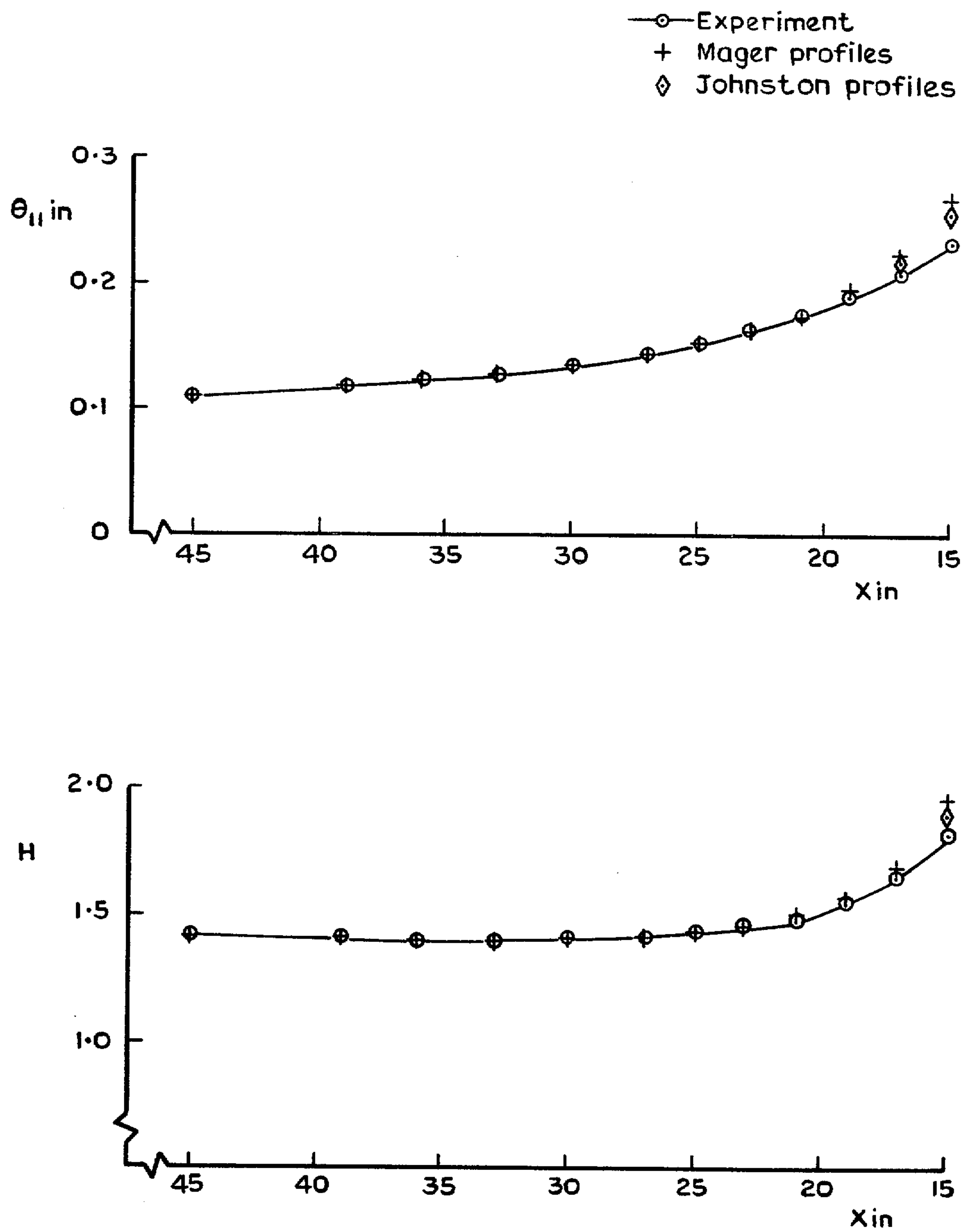

FIG. 4. Johnston flow plane of symmetry streamwise momentum thickness and shape factor.

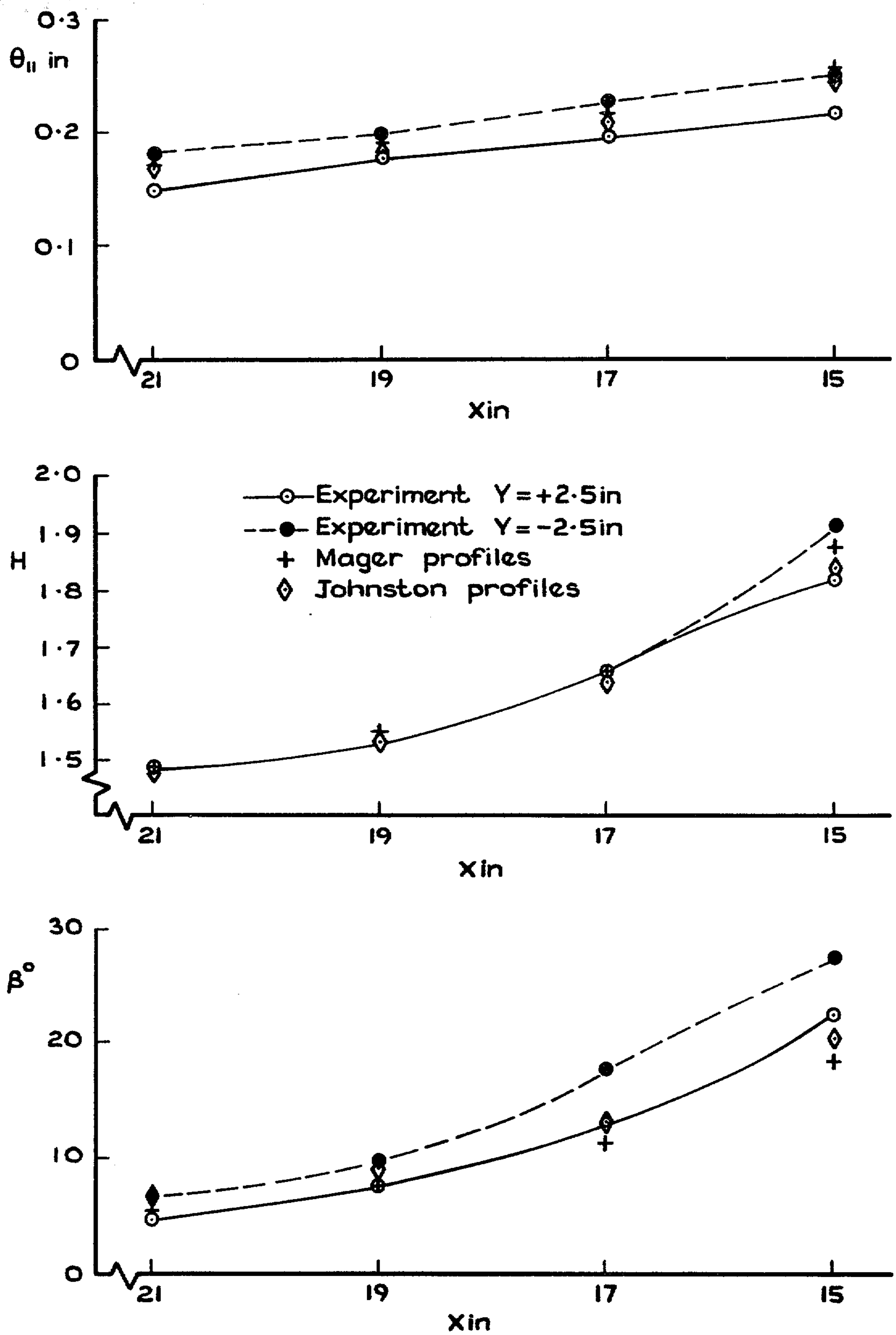

FIG. 5. Johnston flow $Y = \pm 2{\cdot}5$ in. streamwise momentum thickness, shape factor and limiting streamline angle.

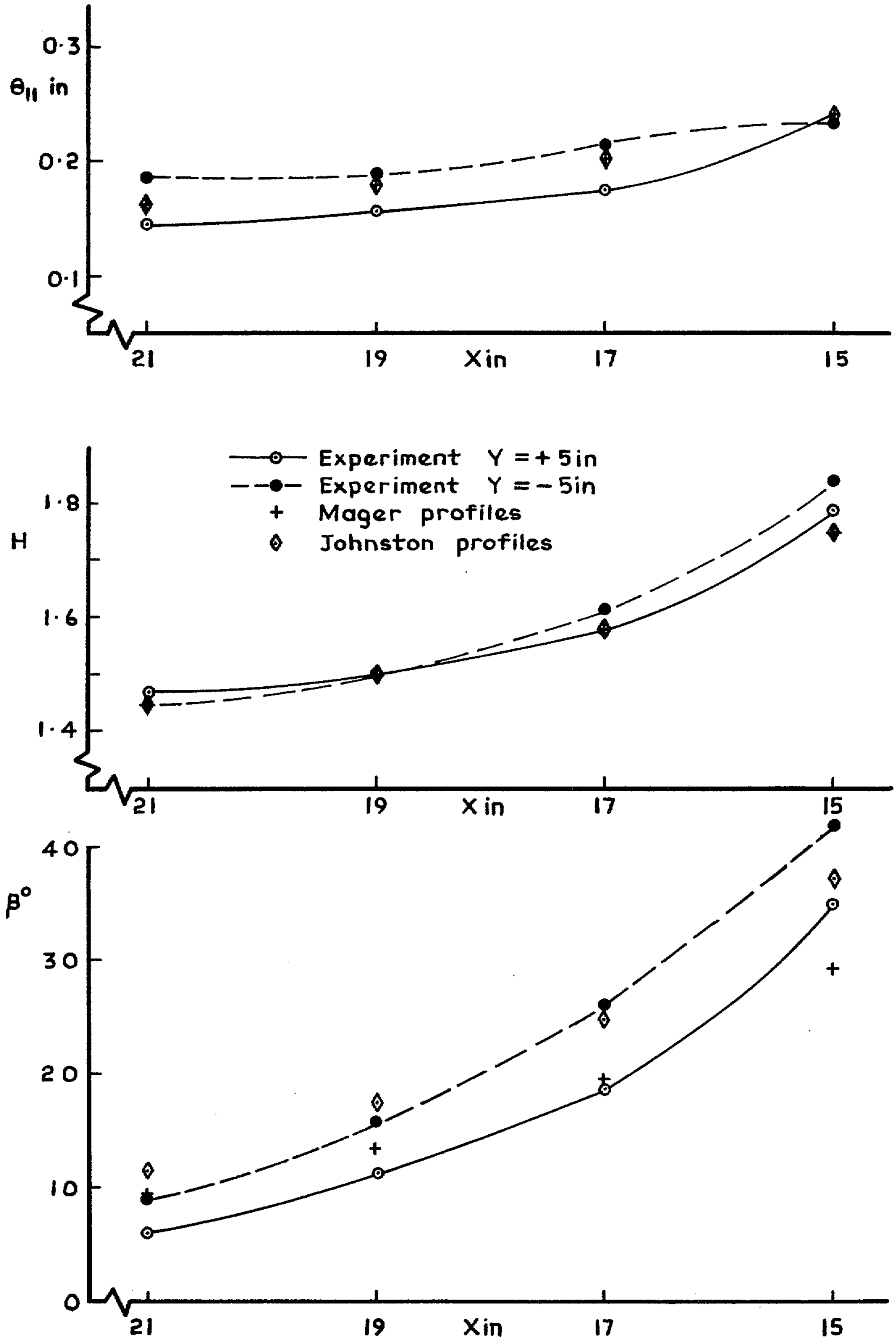

FIG. 6. Johnston flow $Y = \pm 5$ in. streamwise momentum thickness, shape factor and limiting streamline angle.

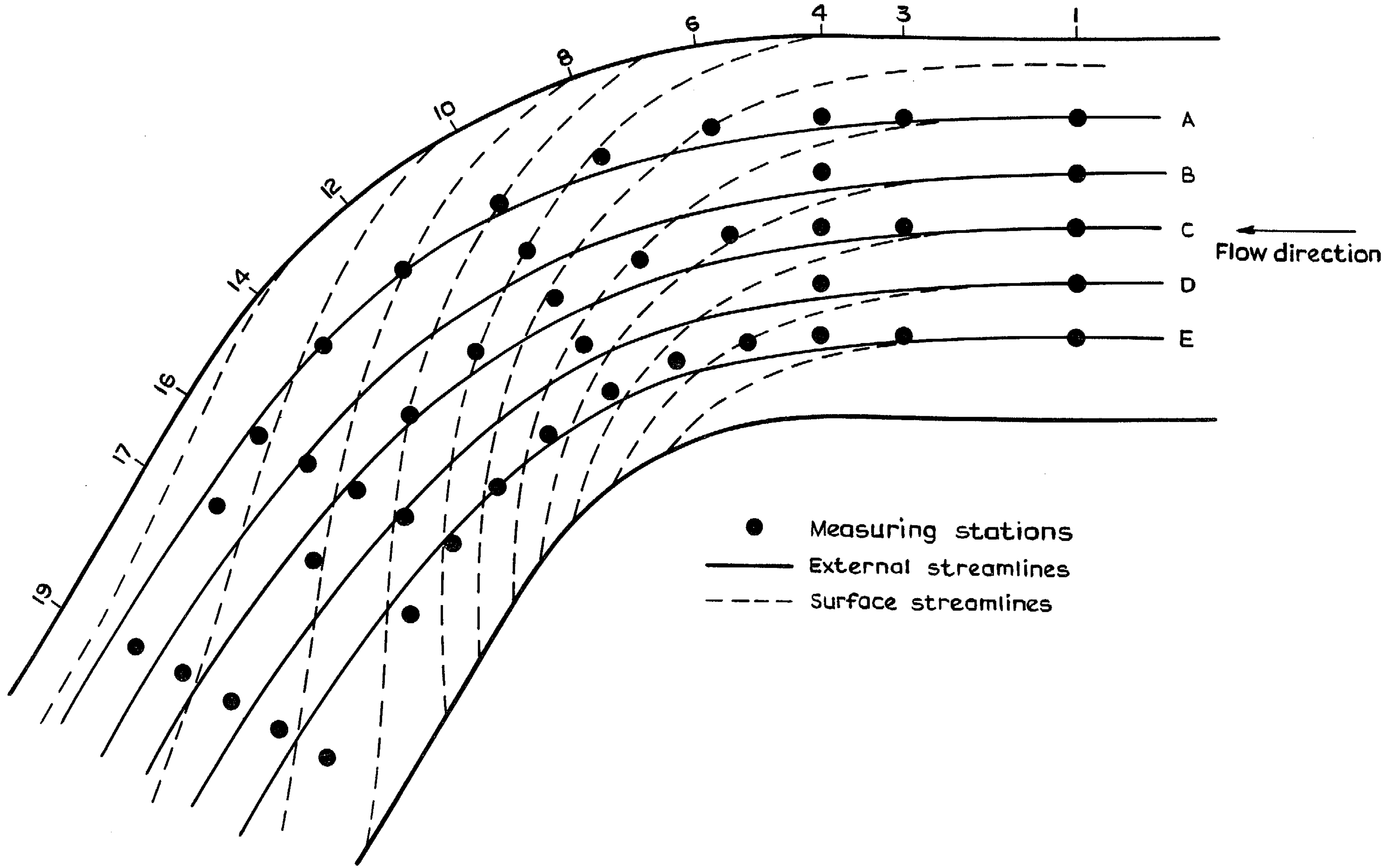

FIG. 7. Vermeulen's experiment series 1.

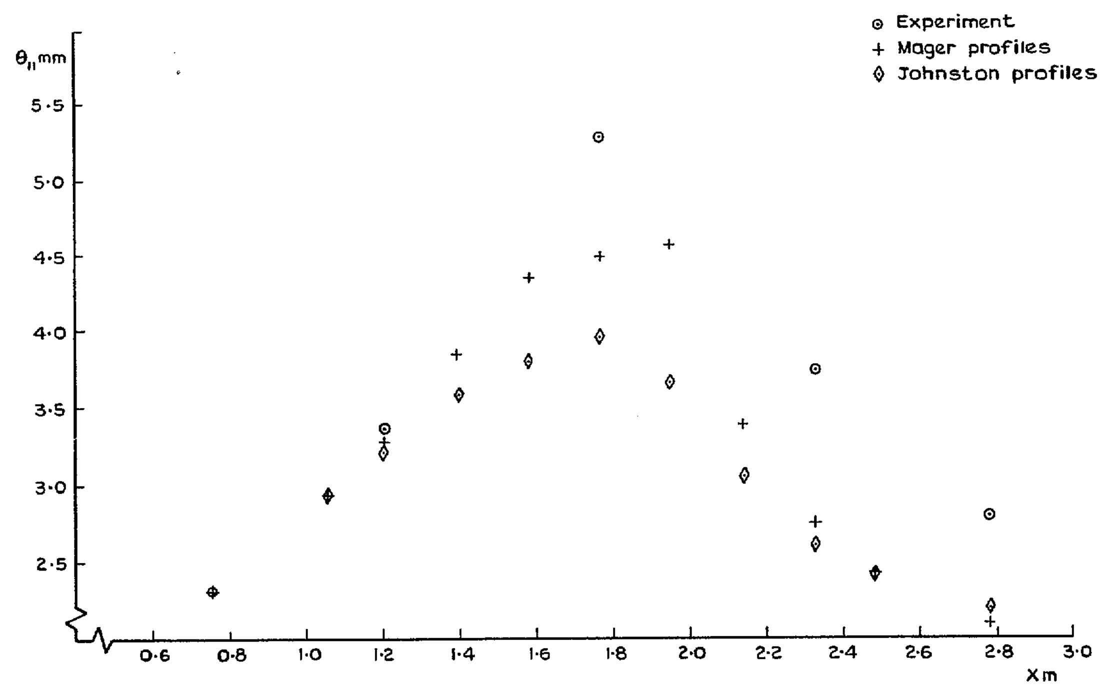

FIG. 8. Vermeulen series 1 line B streamwise momentum thickness.

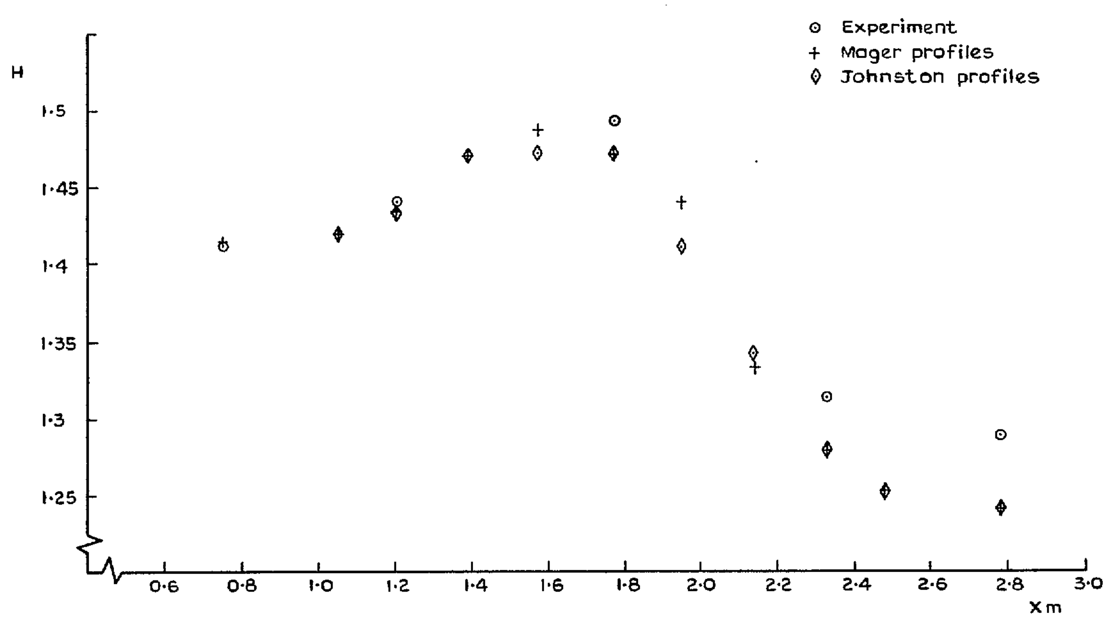

FIG. 9. Vermeulen series 1 line B shape factor.

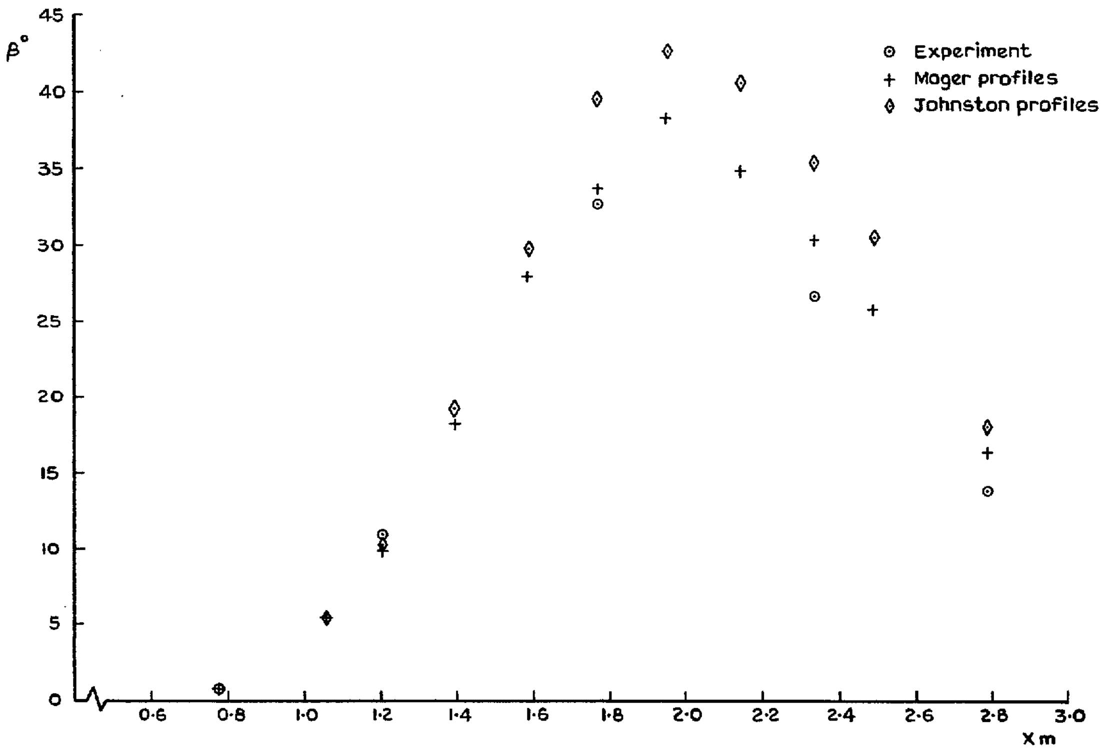

FIG. 10. Vermeulen series 1 line B limiting streamline angle.

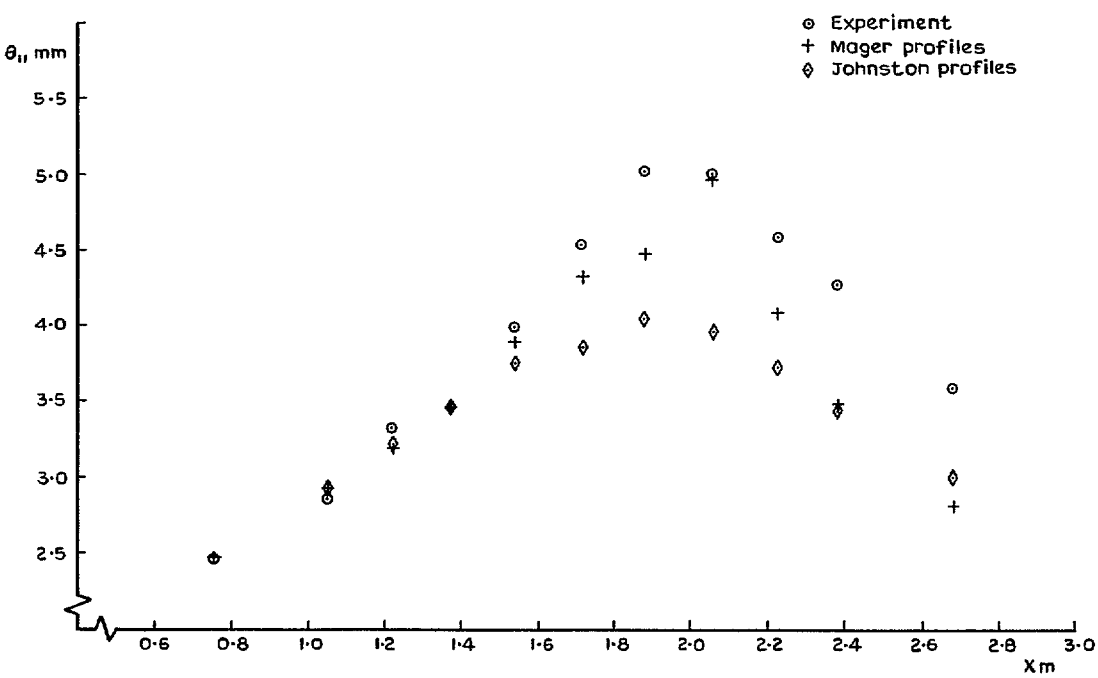

FIG. 11. Vermeulen series 1 line C streamwise momentum thickness.

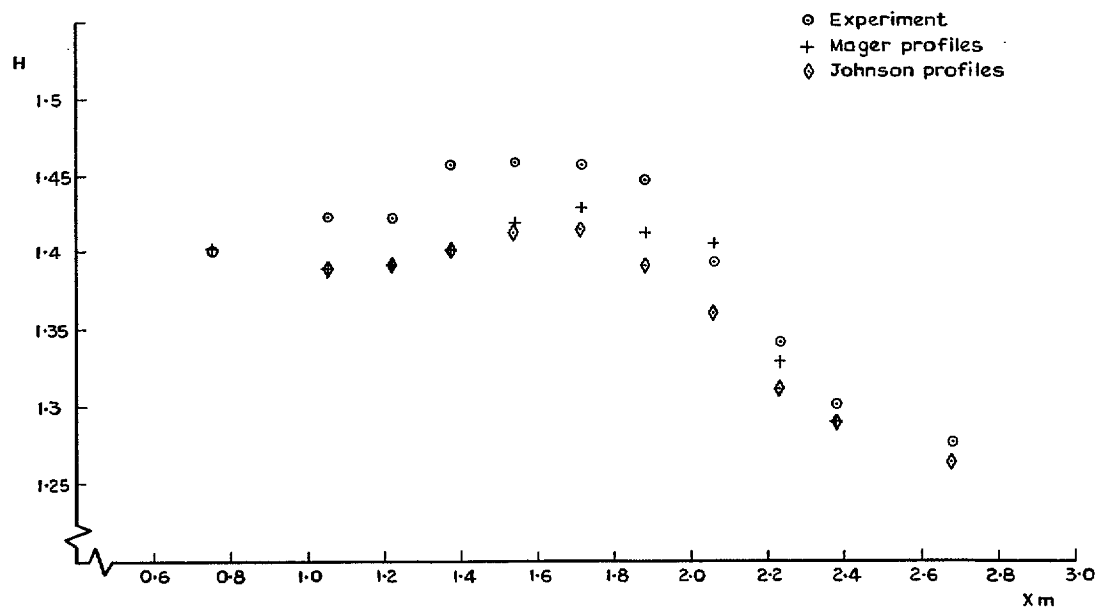

FIG. 12. Vermeulen series 1 line C shape factor.

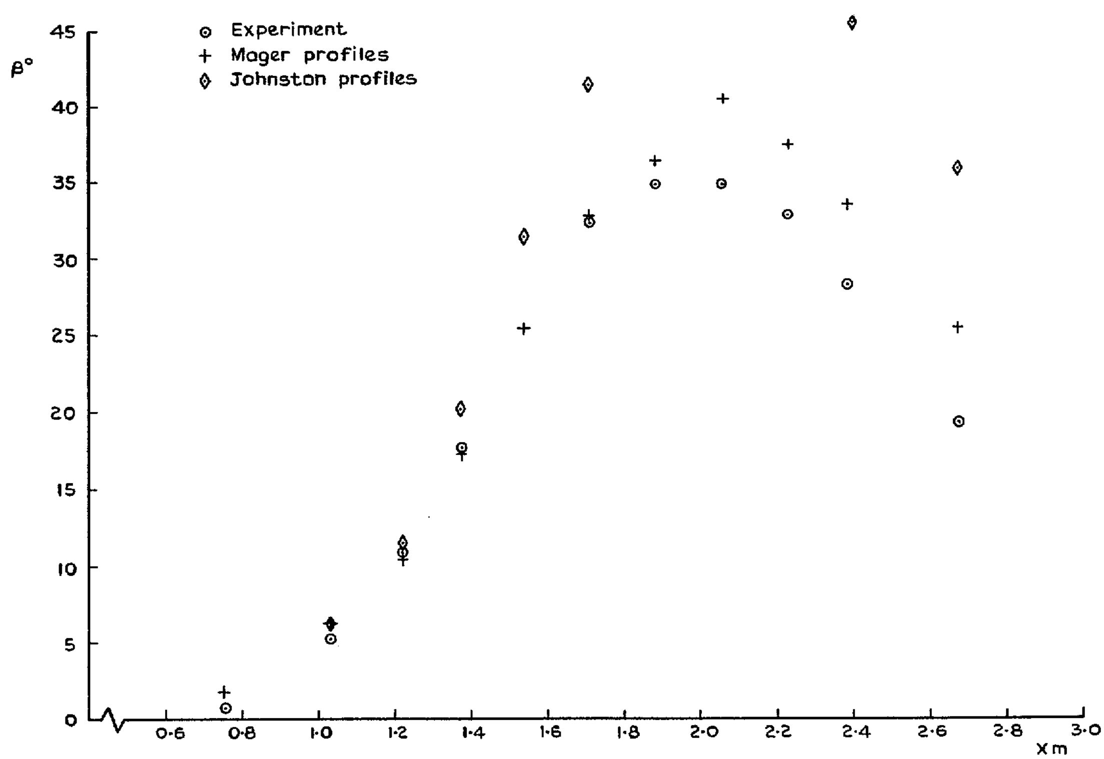

FIG. 13. Vermeulen series 1 line C limiting streamline angle.

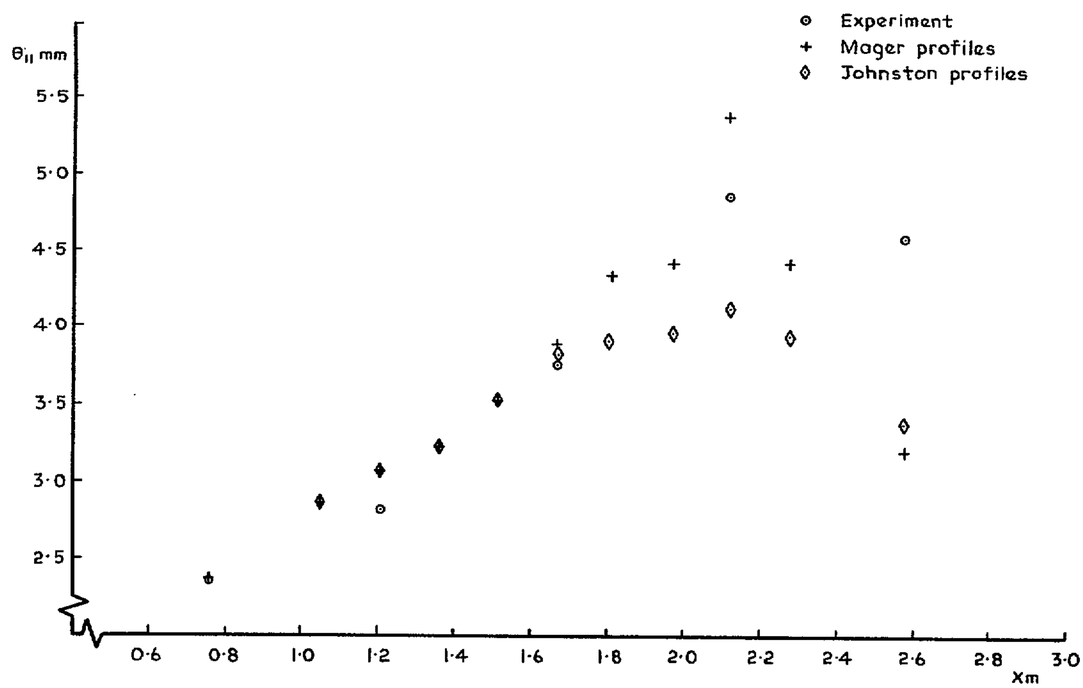

FIG. 14. Vermeulen series 1 line D streamwise momentum thickness.

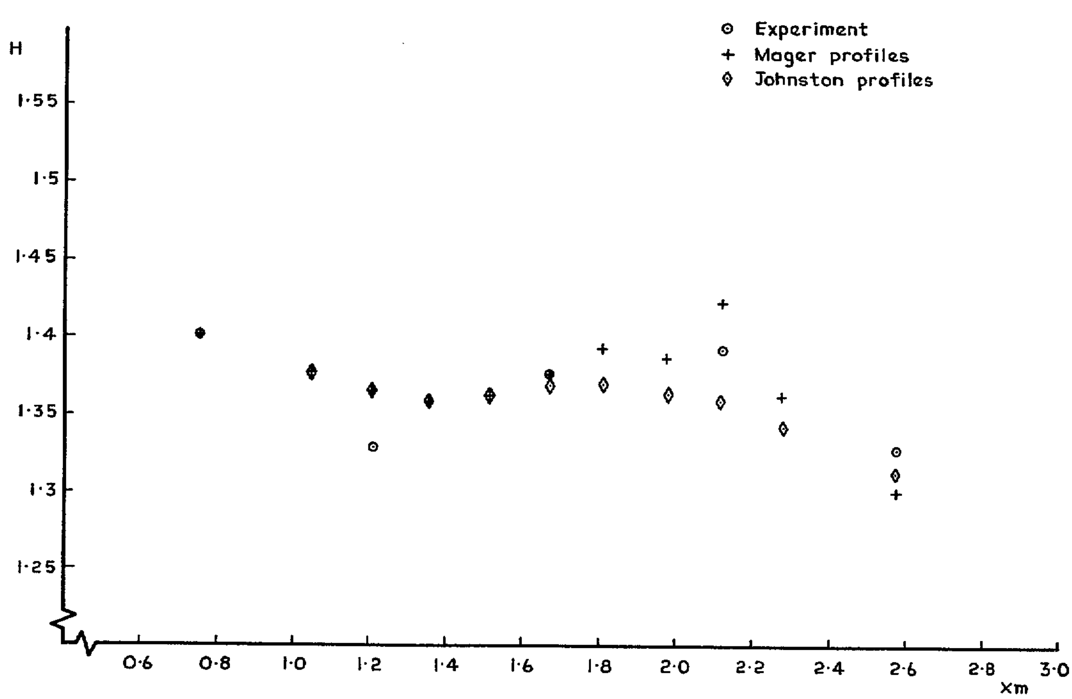

FIG. 15. Vermeulen series 1 line D shape factor.

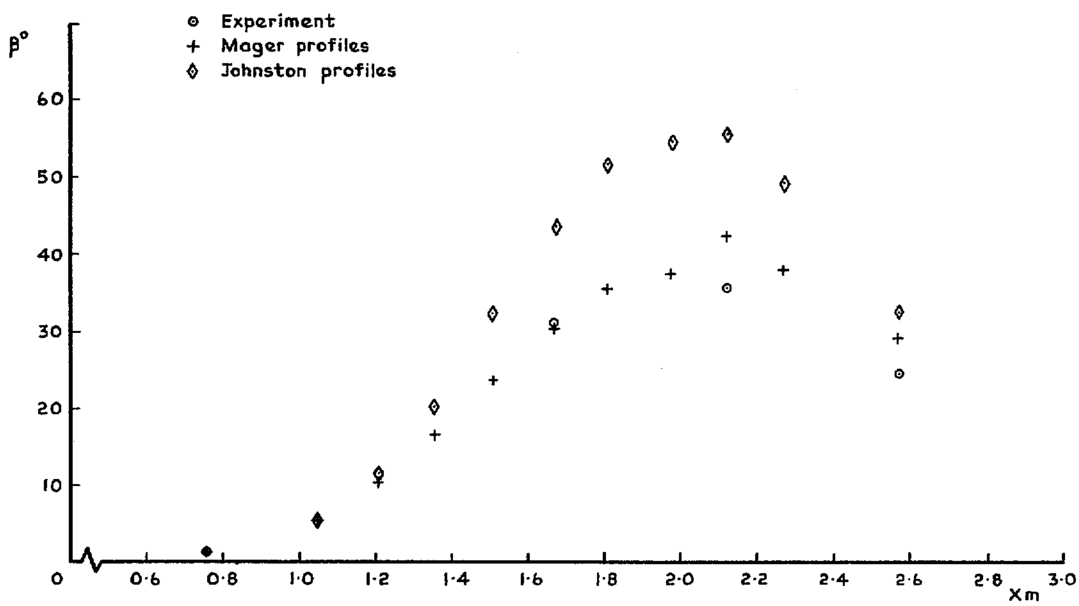

FIG. 16. Vermeulen series 1 line D limiting streamline angle.

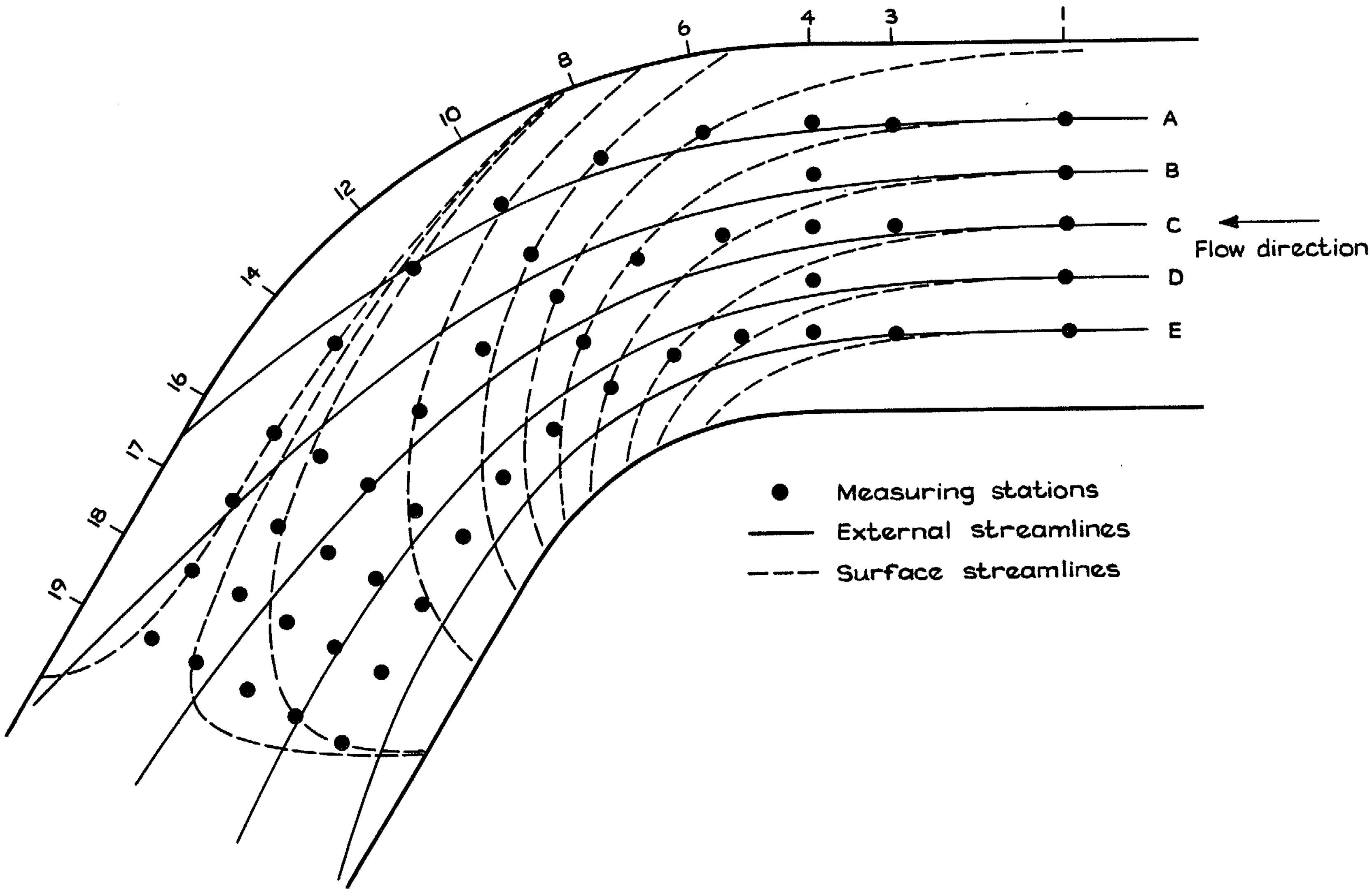

FIG. 17. Vermeulen's experiment series 2.

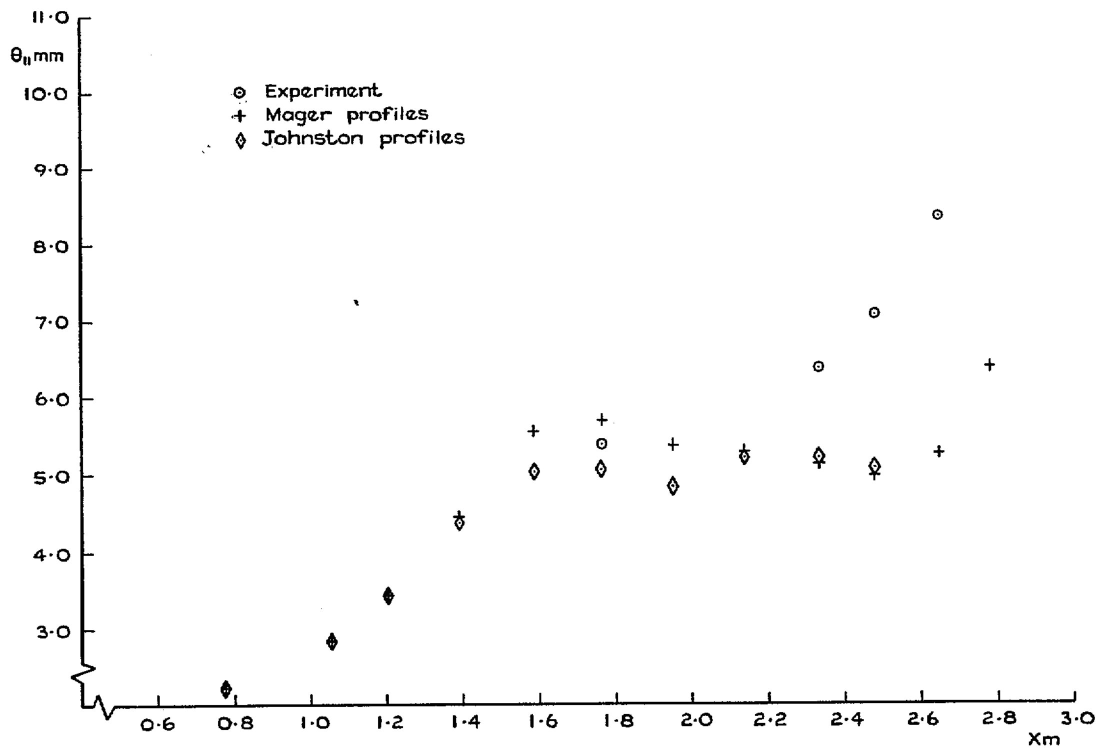

FIG. 18. Vermeulen series 2 line B streamwise momentum thickness.

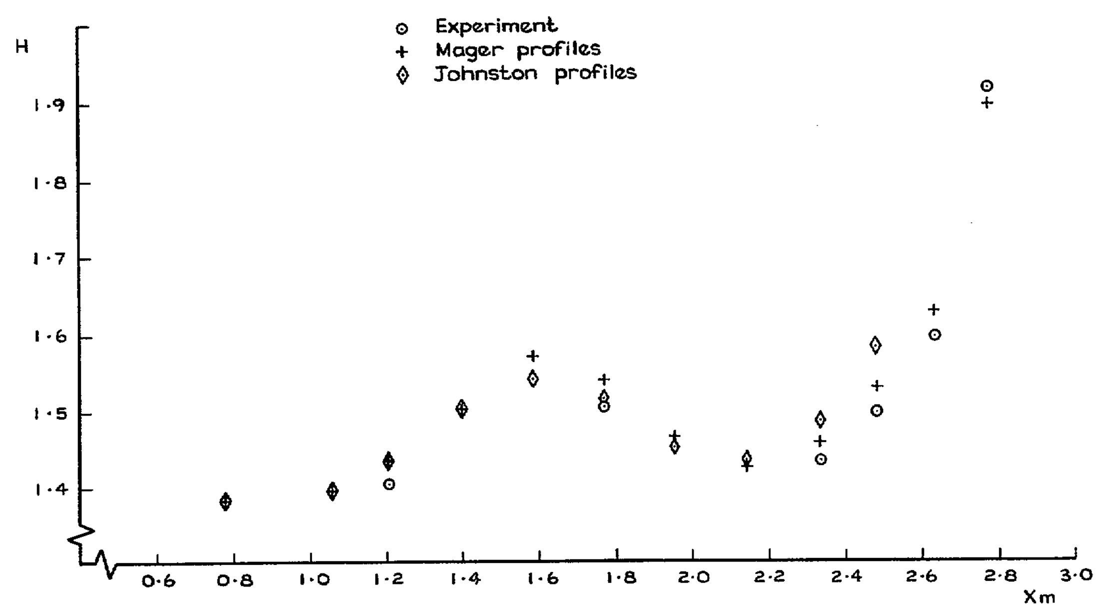

FIG. 19. Vermeulen series 2 line B shape factor.

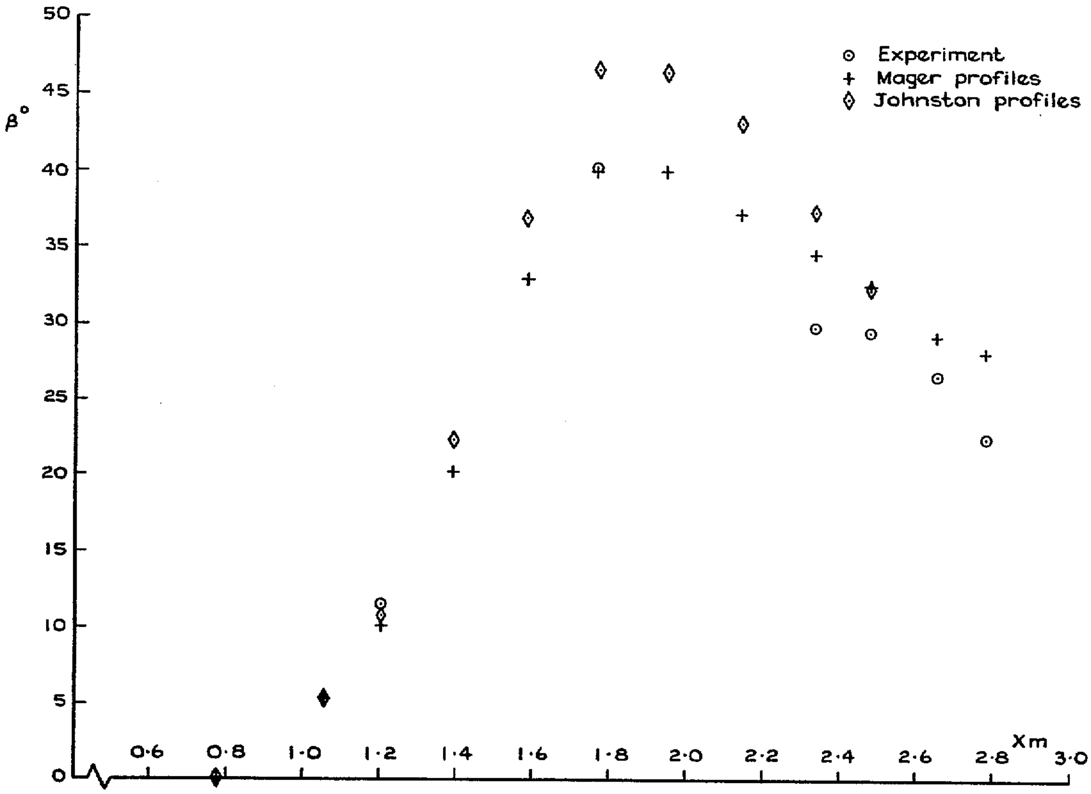

FIG. 20. Vermeulen series 2 line B limiting streamline angle.

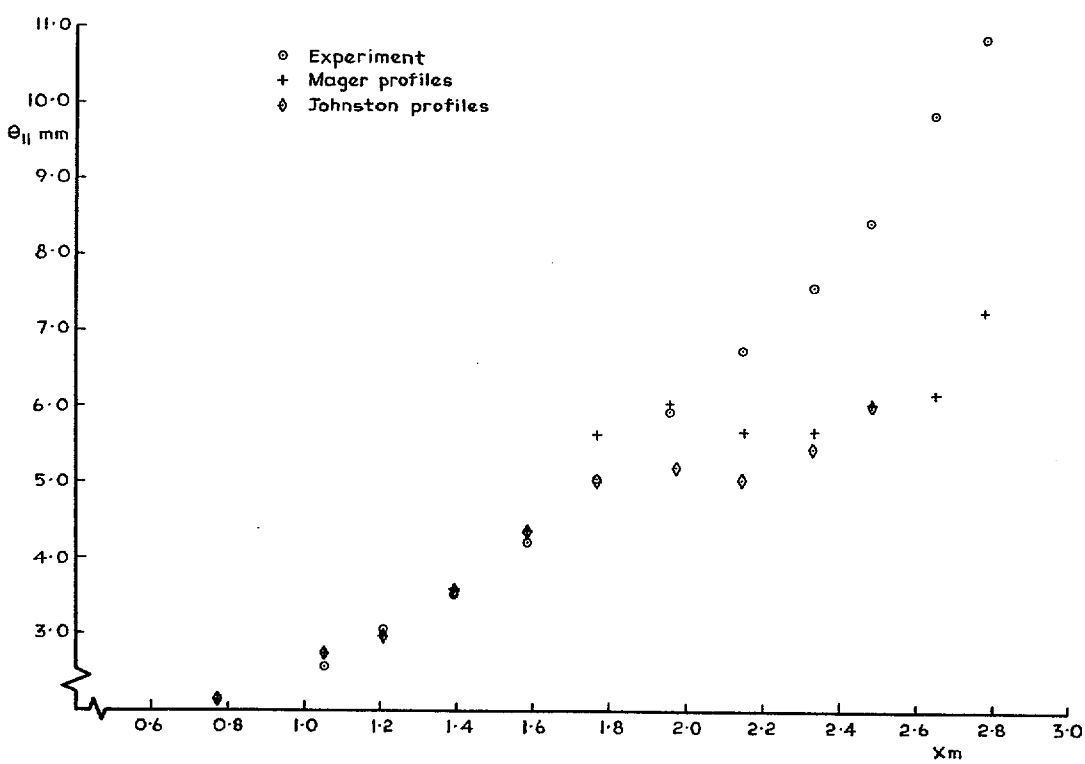

FIG. 21. Vermeulen series 2 line C streamwise momentum thickness.

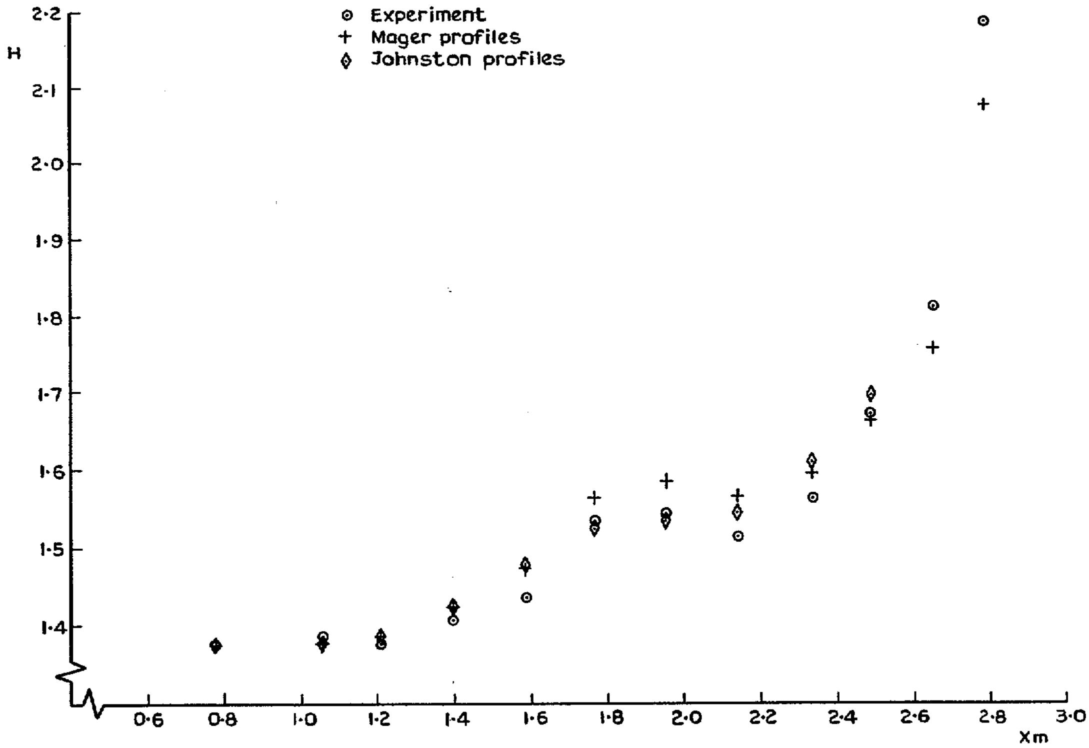

FIG. 22. Vermeulen series 2 line C shape factor.

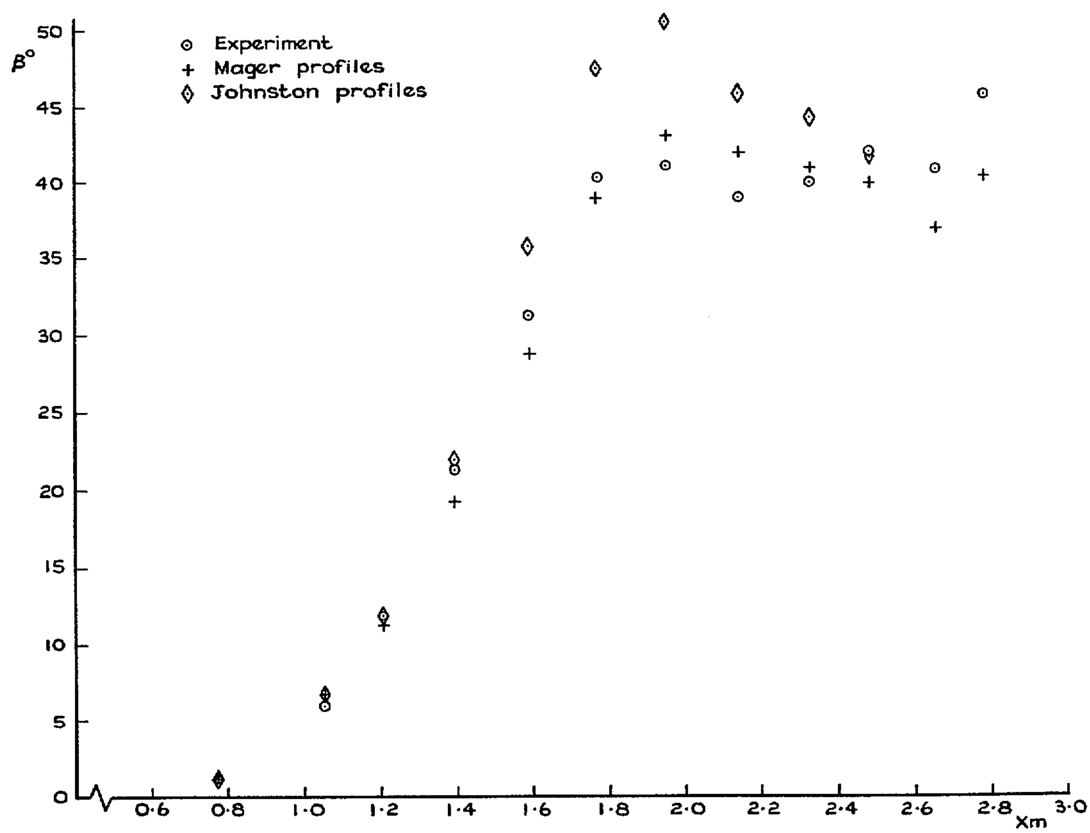

FIG. 23. Vermeulen series 2 line C limiting streamline angle.

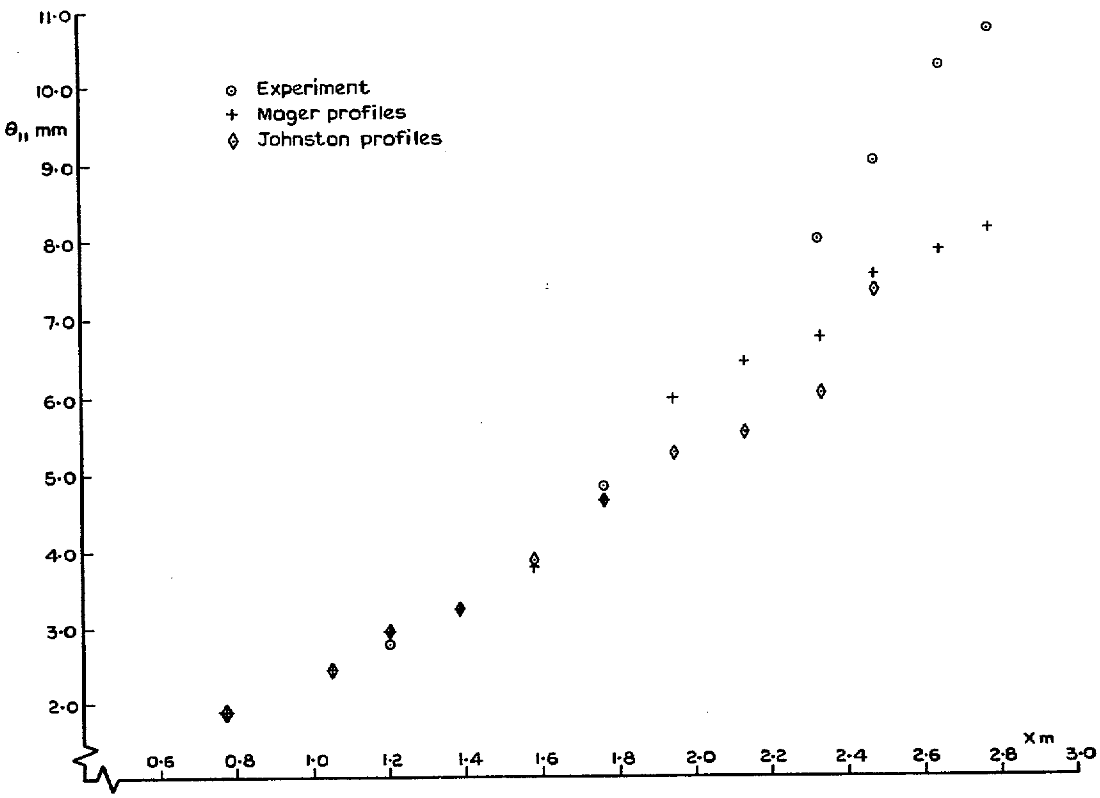

FIG. 24. Vermeulen series 2 line D streamwise momentum thickness.

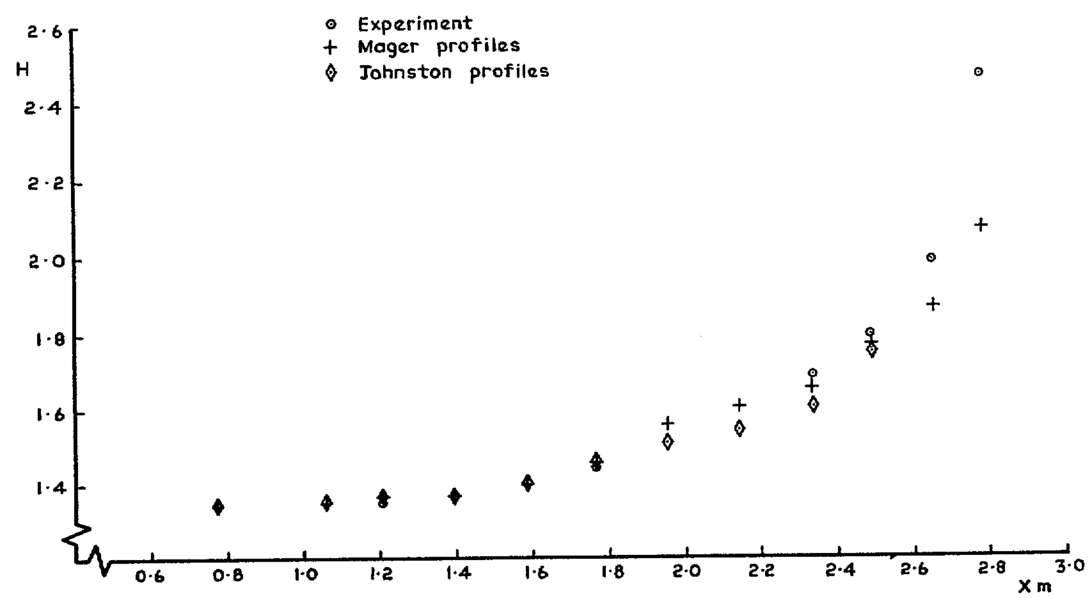

FIG. 25. Vermeulen series 2 line D shape factor.

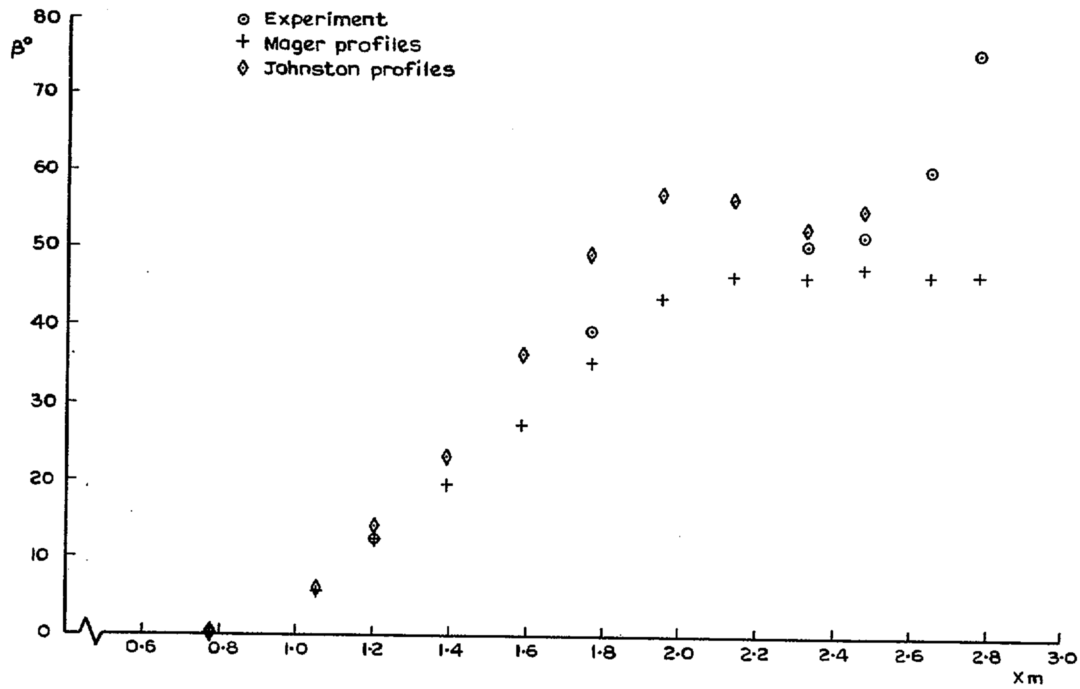

FIG. 26. Vermeulen series 2 line D limiting streamline angle.

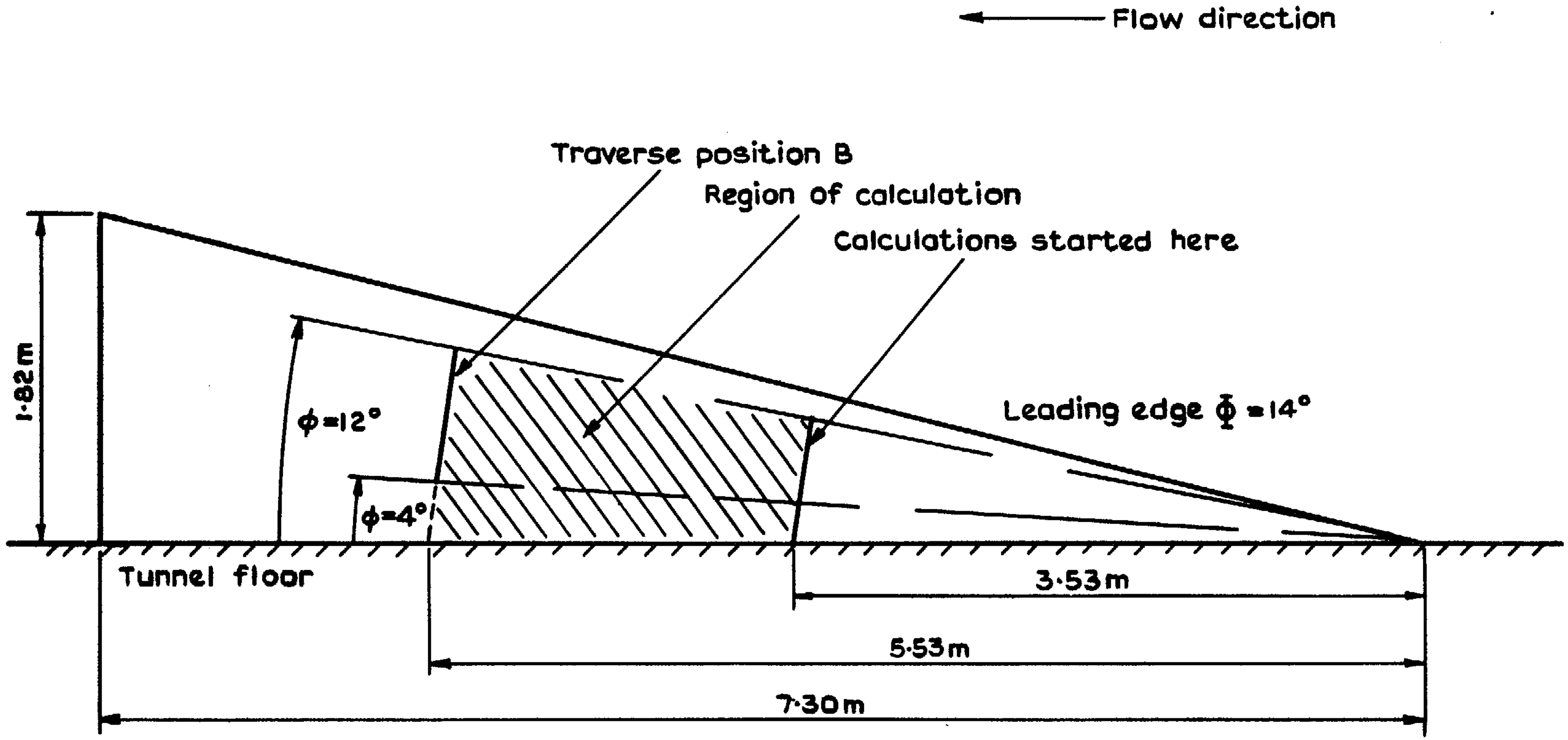

FIG. 27. East's half delta experiment.

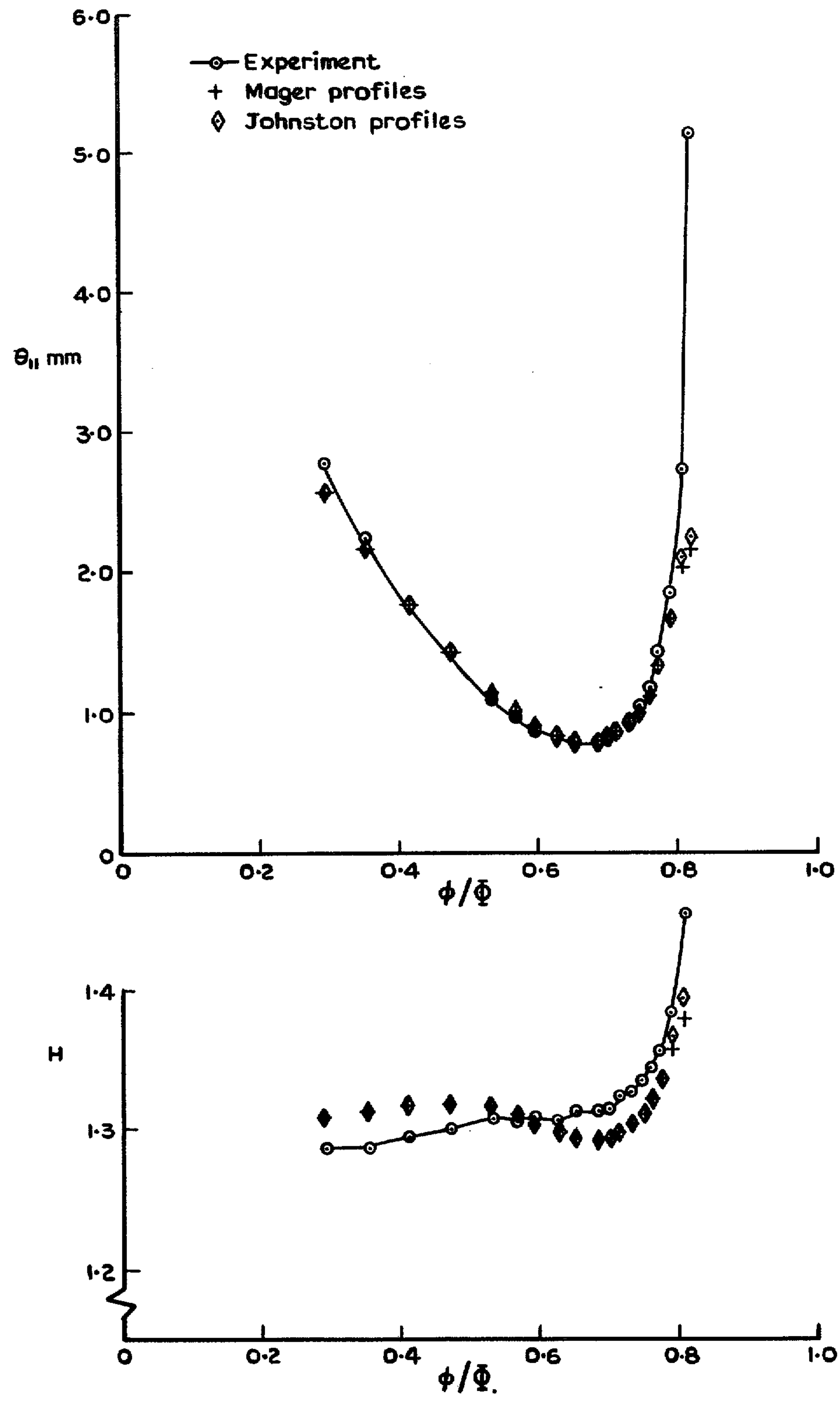

FIG. 28. East's half delta experiment streamwise momentum thickness and shape factor.

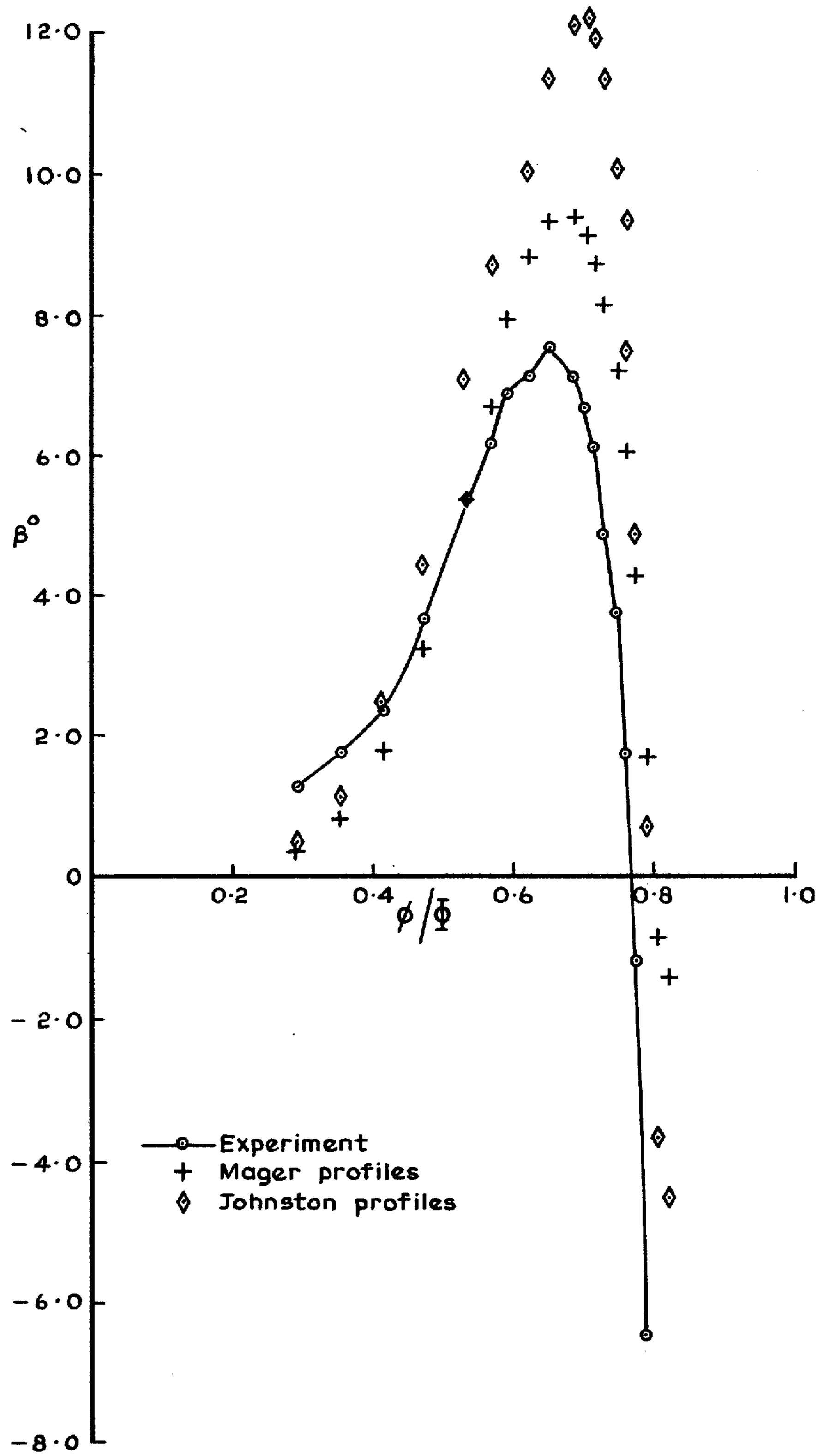

FIG. 29. East's half delta experiment limiting streamline angle.

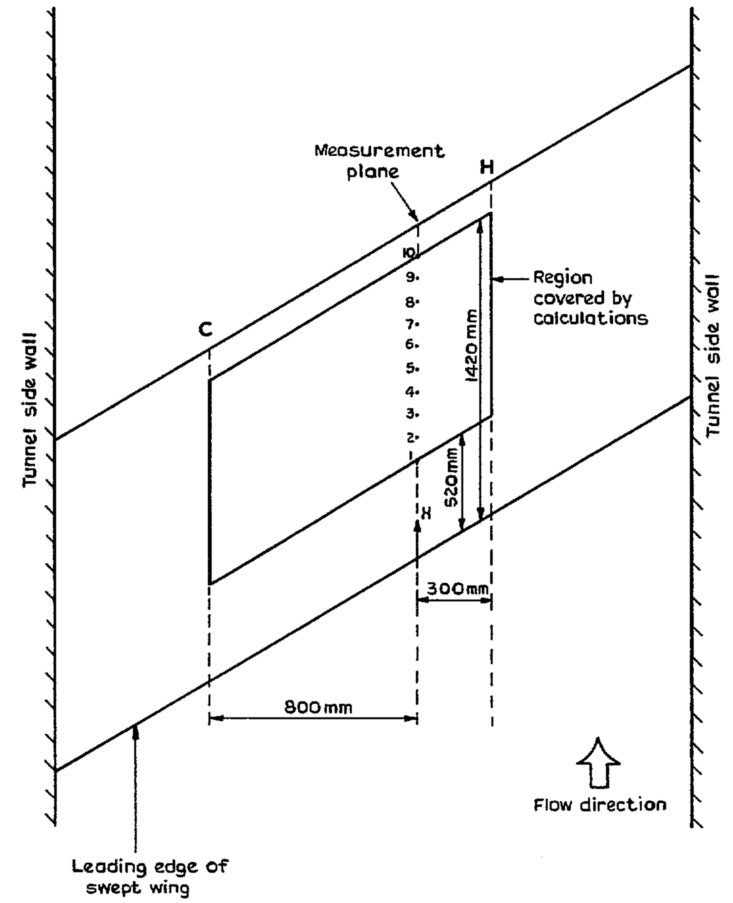

FIG. 30. Van Den Berg and Elsenaar's infinite swept wing.

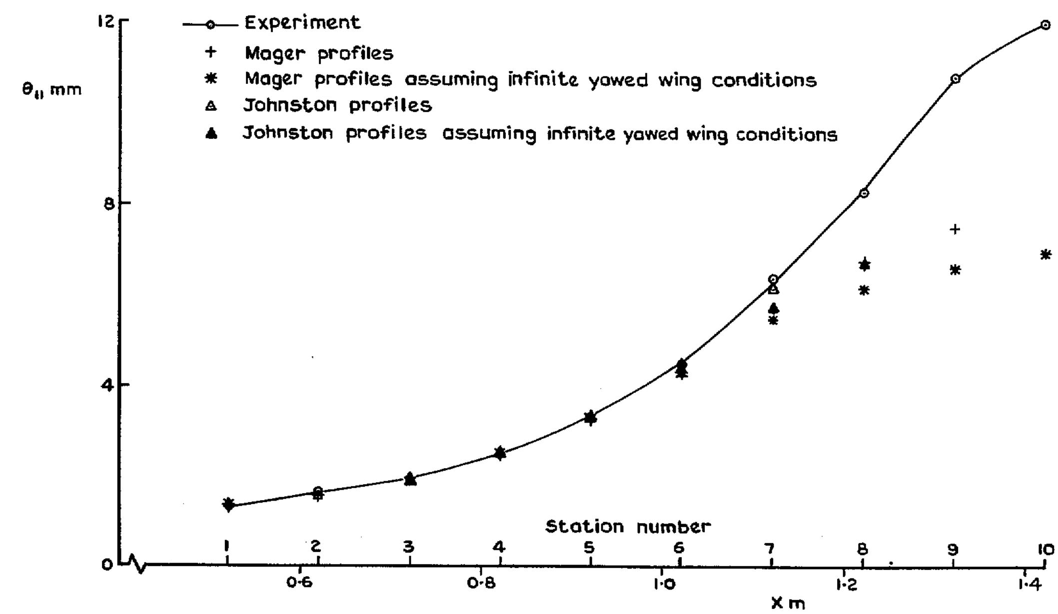

FIG. 31. Van Den Berg and Elsenaar's infinite swept wing streamwise momentum thickness.

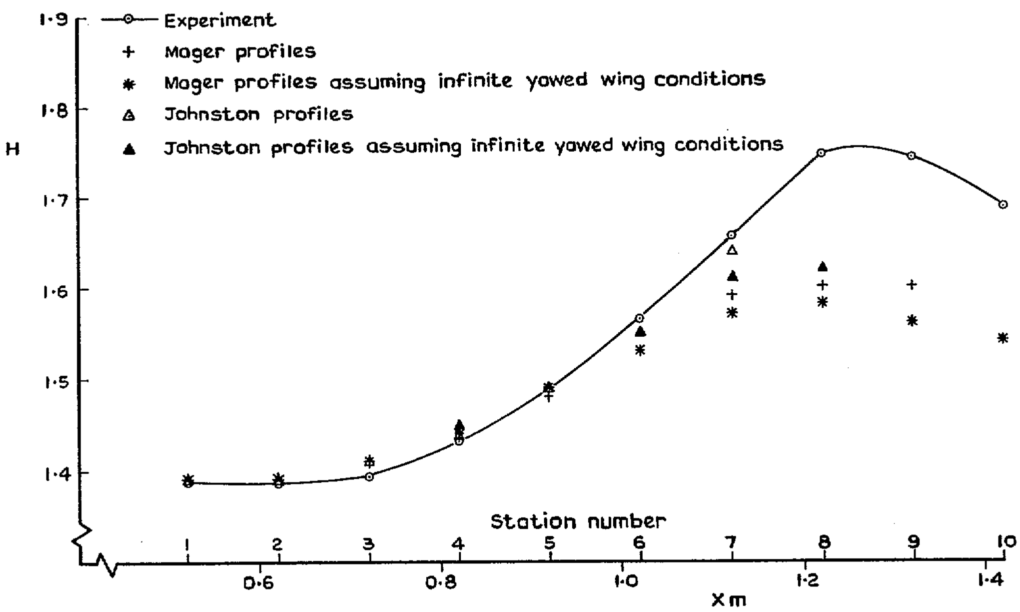

FIG. 32. Van Den Berg and Elsenaar's infinite swept wing shape factor.

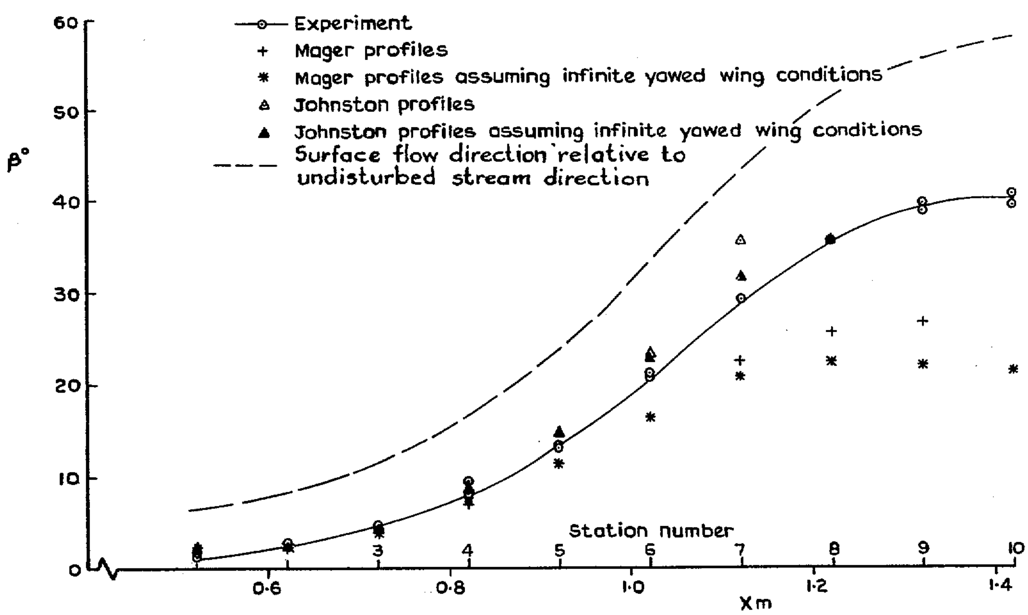

FIG. 33. Van Den Berg and Elsenaar's infinite swept wing limiting streamline angle.

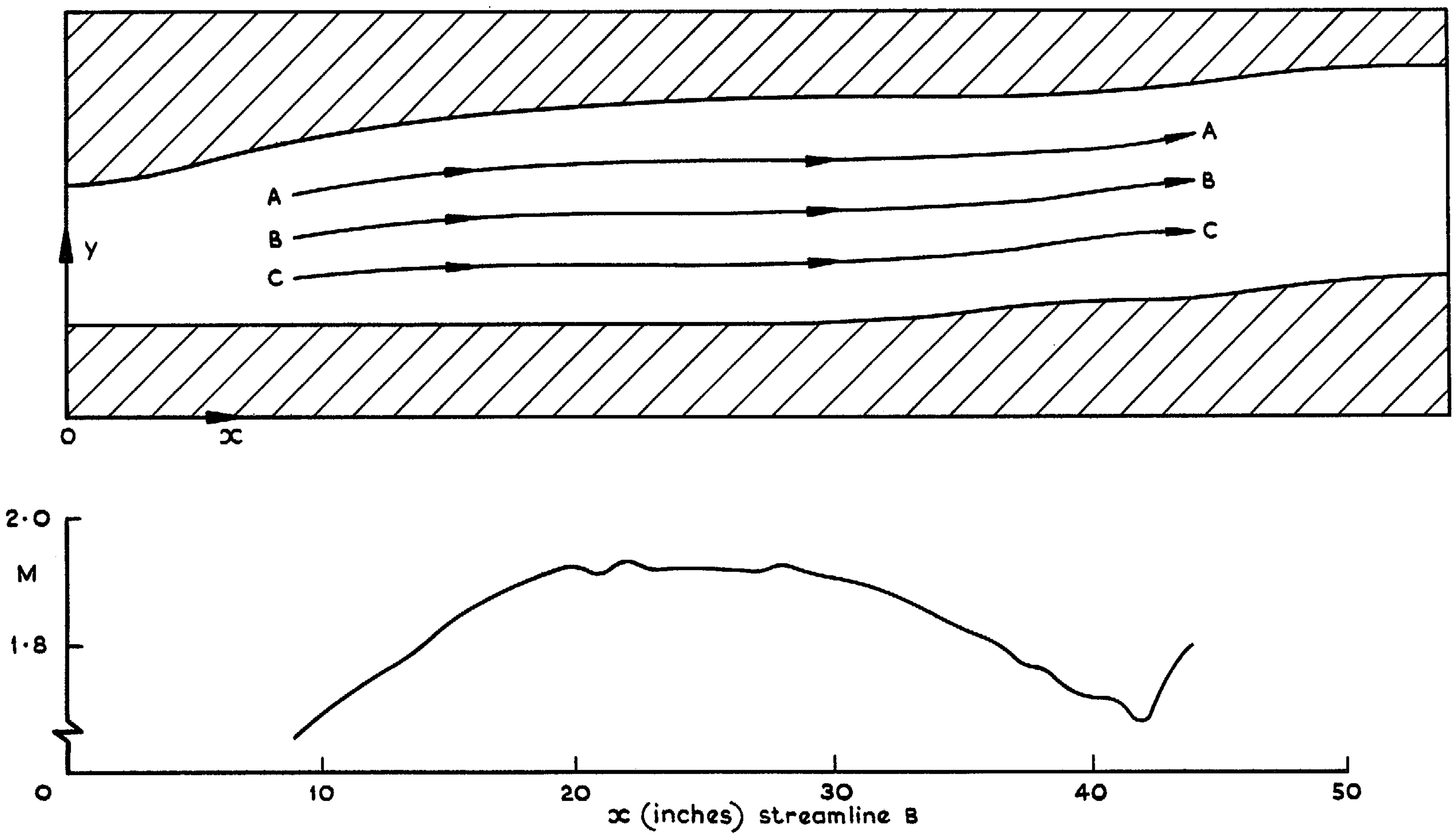

FIG. 34. Hall and Dickens supersonic nozzle external streamlines in test section and Mach number distribution along streamline B.

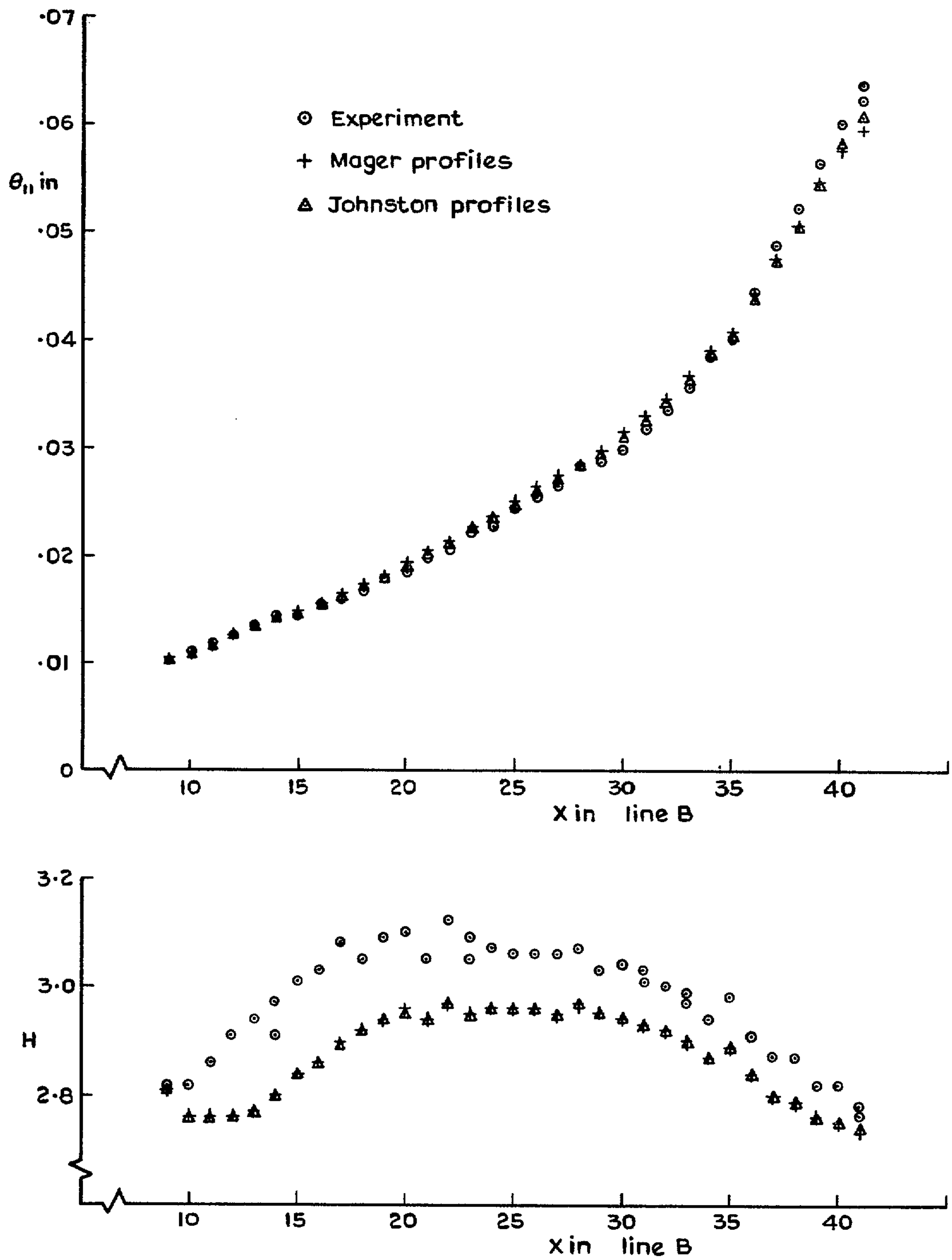

FIG. 35. Hall and Dickens supersonic nozzle streamwise momentum thickness and shape factor.

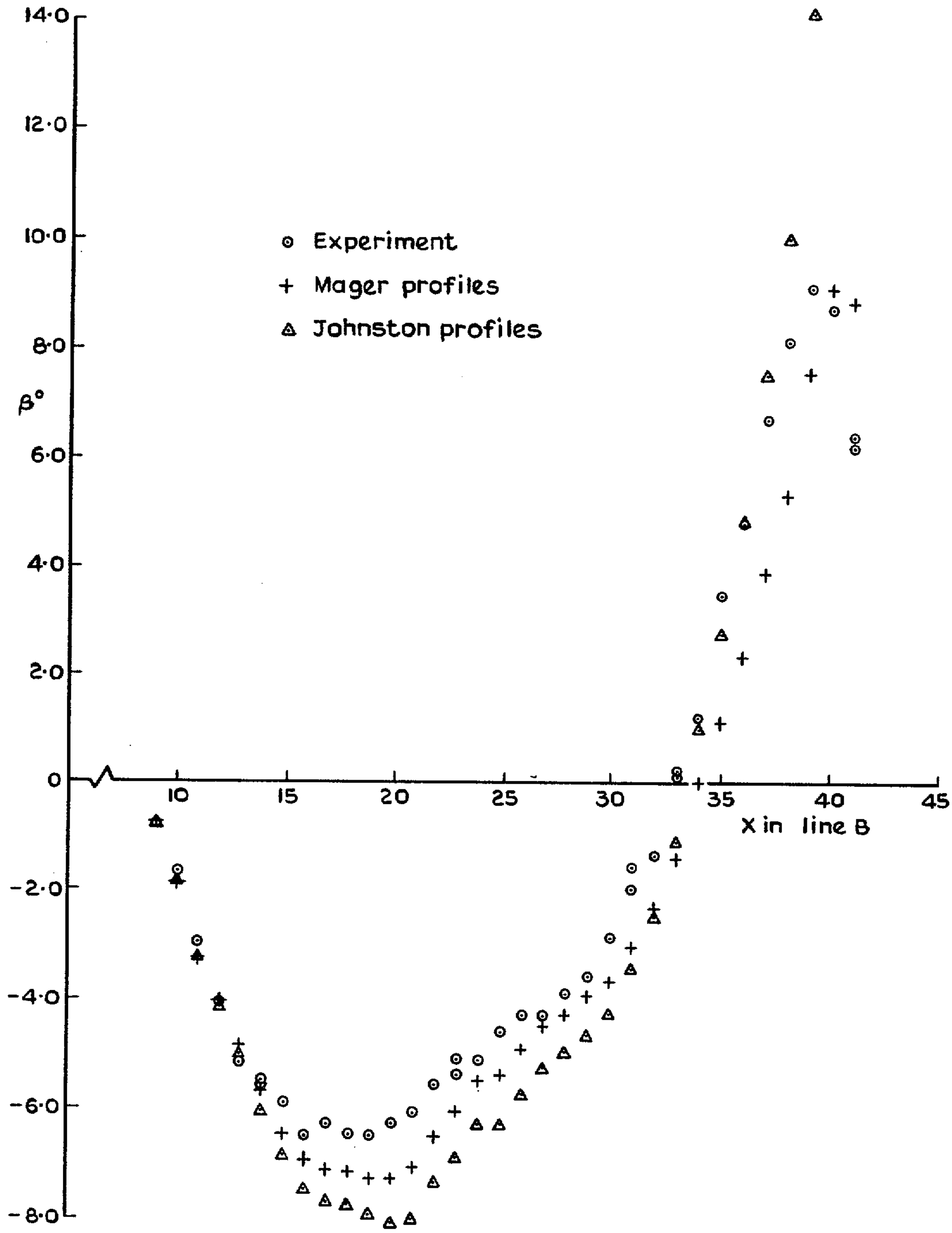

FIG. 36. Hall and Dickens supersonic nozzle limiting streamline angle.

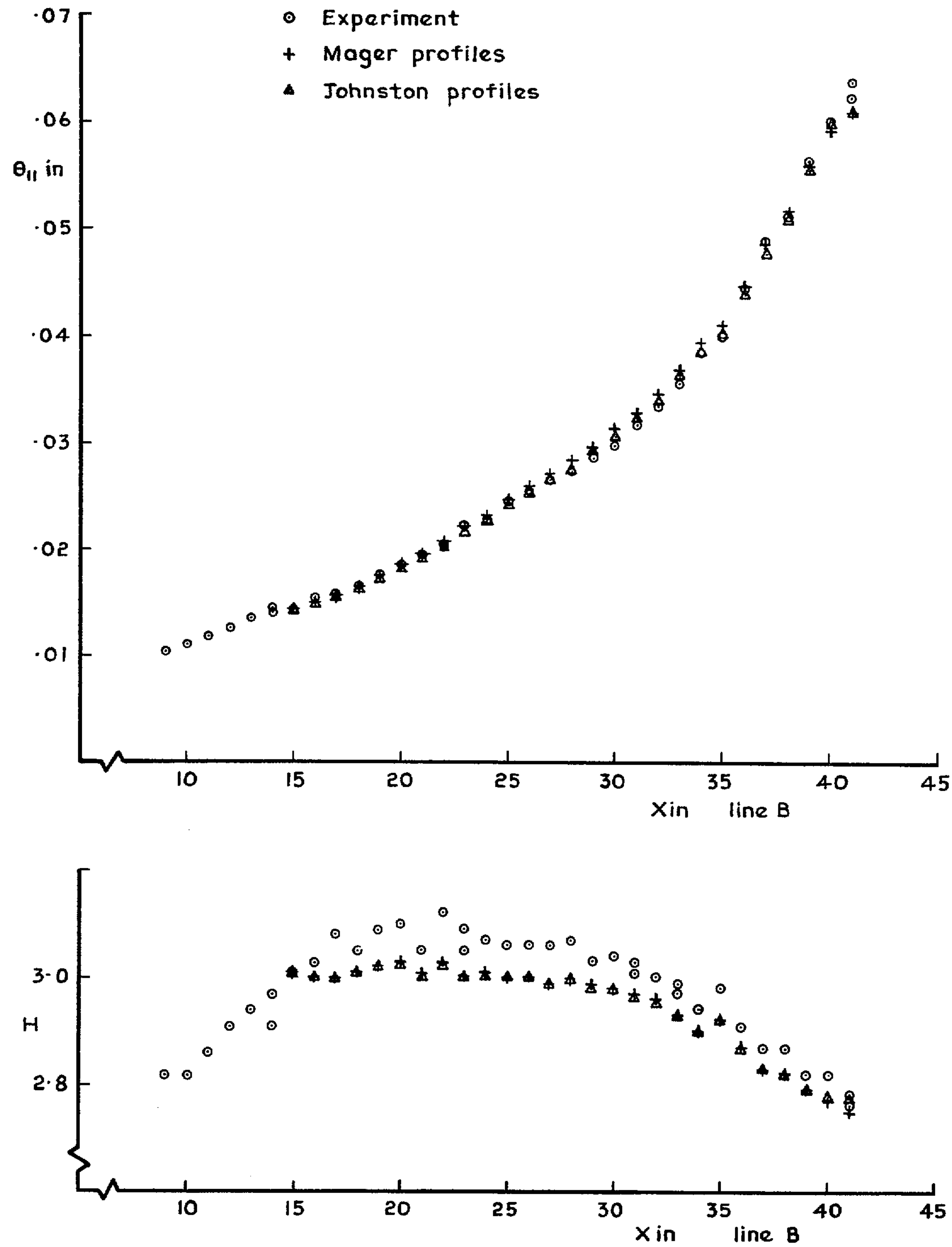

FIG. 37. Hall and Dickens supersonic nozzle streamwise momentum thickness and shape factor calculations started at $X = 15$ in.

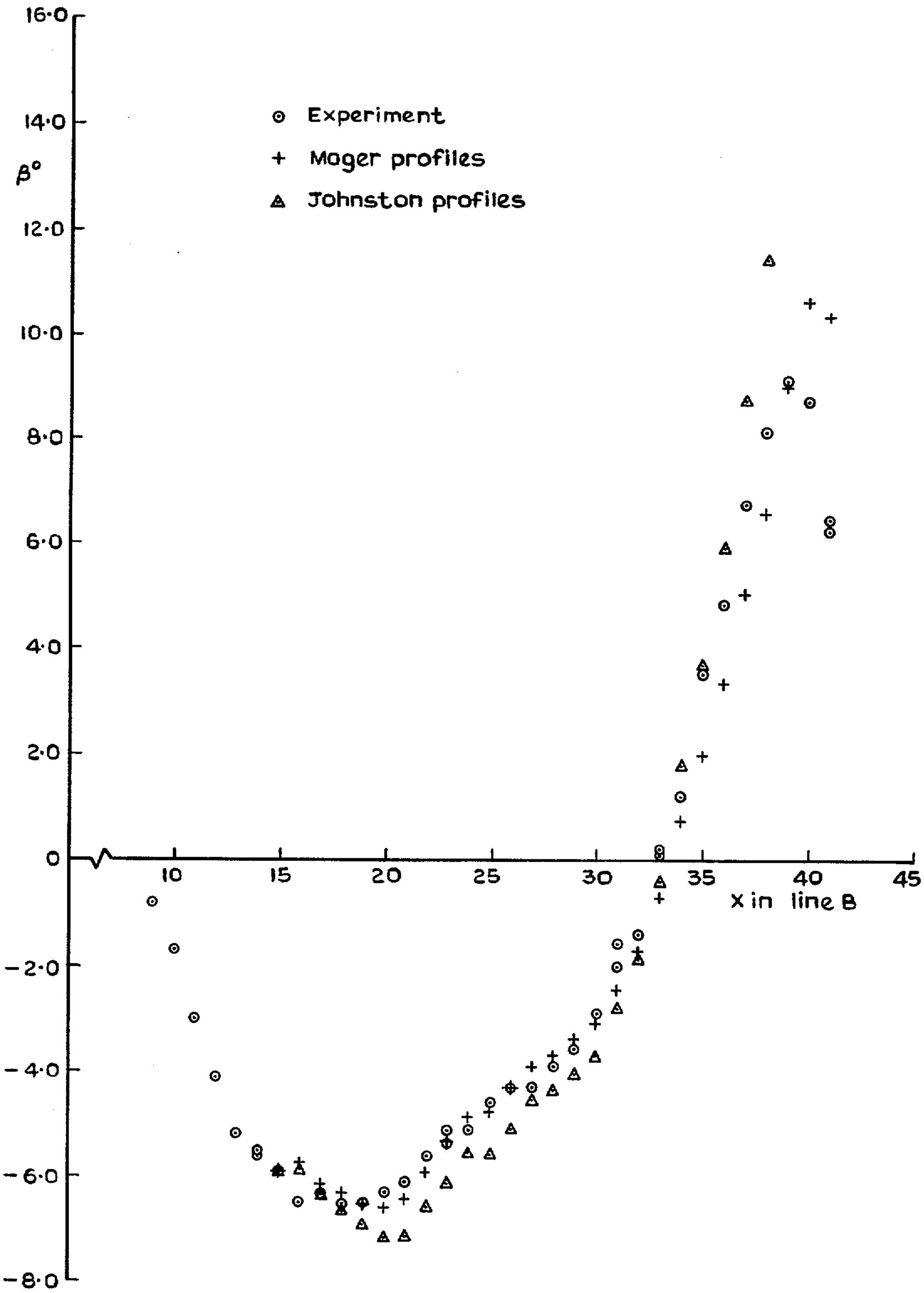

FIG. 38. Hall and Dickens supersonic nozzle limiting streamline angle calculations started at $X = 15$ in.

Printed in England for Her Majesty's Stationery Office by J. W. Arrowsmith Ltd., Bristol BS3 2NT
Dd 505715 1/74

A.R.C. R. & M. No. 3739
December, 1972
P. D. Smith

532.526.4:
533.6.011.34/5

AN INTEGRAL PREDICTION METHOD FOR THREE-DIMENSIONAL COMPRESSIBLE TURBULENT BOUNDARY LAYERS

A calculation method has been developed which uses the compressible forms of the boundary-layer momentum integral and entrainment equations in a general, curvilinear surface coordinate system in which the axes are not necessarily orthogonal. Both the Mager and Johnston representations of the crossflow velocity profile can be used. The set of equations used is hyperbolic and is solved numerically by a simple explicit finite difference method. In cases where the metrics of the

A.R.C. R. & M. No. 3739
December, 1972
P. D. Smith

532.526.4:
533.6.011.34/5

AN INTEGRAL PREDICTION METHOD FOR THREE-DIMENSIONAL COMPRESSIBLE TURBULENT BOUNDARY LAYERS

A calculation method has been developed which uses the compressible forms of the boundary-layer momentum integral and entrainment equations in a general, curvilinear surface coordinate system in which the axes are not necessarily orthogonal. Both the Mager and Johnston representations of the crossflow velocity profile can be used. The set of equations used is hyperbolic and is solved numerically by a simple explicit finite difference method. In cases where the metrics of the

A.R.C. R. & M. No. 3739
December, 1972
P. D. Smith

532.526.4:
533.6.011.34/5

AN INTEGRAL PREDICTION METHOD FOR THREE-DIMENSIONAL COMPRESSIBLE TURBULENT BOUNDARY LAYERS

A calculation method has been developed which uses the compressible forms of the boundary-layer momentum integral and entrainment equations in a general, curvilinear surface coordinate system in which the axes are not necessarily orthogonal. Both the Mager and Johnston representations of the crossflow velocity profile can be used. The set of equations used is hyperbolic and is solved numerically by a simple explicit finite difference method. In cases where the metrics of the

A.R.C. R. & M. No. 3739
December, 1972
P. D. Smith

532.526.4:
533.6.011.34/5

AN INTEGRAL PREDICTION METHOD FOR THREE-DIMENSIONAL COMPRESSIBLE TURBULENT BOUNDARY LAYERS

A calculation method has been developed which uses the compressible forms of the boundary-layer momentum integral and entrainment equations in a general, curvilinear surface coordinate system in which the axes are not necessarily orthogonal. Both the Mager and Johnston representations of the crossflow velocity profile can be used. The set of equations used is hyperbolic and is solved numerically by a simple explicit finite difference method. In cases where the metrics of the

coordinate system used are not known analytically a method is given for obtaining them from the cartesian coordinates of the surface. A method is also presented for determining the external velocity field from a given pressure distribution. Comparisons are given of predictions of the boundary-layer method with the experimental results of Johnston, Vermeulen, East, van den Berg and Elsenaar, and Hall and Dickens. These results, involving five different coordinate systems, were all obtained using the same computer program.

coordinate system used are not known analytically a method is given for obtaining them from the cartesian coordinates of the surface. A method is also presented for determining the external velocity field from a given pressure distribution. Comparisons are given of predictions of the boundary-layer method with the experimental results of Johnston, Vermeulen, East, van den Berg and Elsenaar, and Hall and Dickens. These results, involving five different coordinate systems, were all obtained using the same computer program.

coordinate system used are not known analytically a method is given for obtaining them from the cartesian coordinates of the surface. A method is also presented for determining the external velocity field from a given pressure distribution. Comparisons are given of predictions of the boundary-layer method with the experimental results of Johnston, Vermeulen, East, van den Berg and Elsenaar, and Hall and Dickens. These results, involving five different coordinate systems, were all obtained using the same computer program.

coordinate system used are not known analytically a method is given for obtaining them from the cartesian coordinates of the surface. A method is also presented for determining the external velocity field from a given pressure distribution. Comparisons are given of predictions of the boundary-layer method with the experimental results of Johnston, Vermeulen, East, van den Berg and Elsenaar, and Hall and Dickens. These results, involving five different coordinate systems, were all obtained using the same computer program.

R. & M. No. 3739

HER MAJESTY'S STATIONERY OFFICE

Government Bookshops

49 High Holborn, London WC1V 6HB
13a Castle Street, Edinburgh EH2 3AR
41 The Hayes, Cardiff CF1 1JW
Brazennose Street, Manchester M60 8AS
Southey House, Wine Street, Bristol BS1 2BQ
258 Broad Street, Birmingham B1 2HE
80 Chichester Street, Belfast BT1 4JY

Government publications are also available through booksellers

R. & M. No. 3739
ISBN 0 11 470832 0